



Treball Final de Grau

Coordination compounds derived from R-phenylcyanamido ligands and cobalt (II).

Compostos de coordinació derivats de lligands R-fenilcianamida amb cobalt (II).

Ànnia Tubau Ribot

January 2019



UNIVERSITAT DE
BARCELONA

B:KC Barcelona
Knowledge
Campus
Campus d'Excel·lència Internacional

Aquesta obra esta subjecta a la llicència de:
Reconeixement–NoComercial–SenseObraDerivada



<http://creativecommons.org/licenses/by-nc-nd/3.0/es/>

*Defèn el teu dret a pensar, perquè inclús pensar
de manera errònia és millor que no pensar.*

Hipàtia d' Alexandria.

Gràcies, a la Dra. Saskia Speed Castro, tutora del treball, i al Dr. Ramon Vicente Castillo per guiar-me i aconsellar-me durant el procés d'aprenentatge i realització del treball.

Als meus amics i companys i la meva família, especialment al meu pare.

REPORT

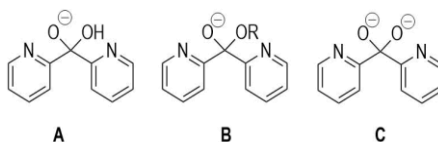
CONTENTS

1. SUMMARY	3
2. RESUM	5
3. INTRODUCTION	7
3.1. Di(2-pyridil) ketone chemistry	7
3.2. R-phenylcyanamides chemistry	9
3.3. Magnetism	9
3.3.1. Lanthanides magnetic properties	11
3.3.3. Single molecule magnets (SMM)	12
4. OBJECTIVES	13
5. RESULTS AND DISCUSSION	13
5.1. IR spectroscopy	13
5.2. Crystal structures	14
5.2.1. Crystal structure of $[\text{Co}_4(\mu_3\text{-py}_2\text{C}(\text{OH})\text{O})_4(4\text{-Br-3-CF}_3\text{-PhNCN})_2(\text{PhCOO})_2]$ (1)	14
5.2.2. Crystal structure of $[\text{Co}_4(\mu_2\text{-py}_2\text{C}(\text{OH})\text{O})_2(\mu_3\text{-py}_2\text{C}(\text{OCH}_3)\text{O})_2(\mu_2\text{-4-Cl-PhNCN})_2(4\text{-Cl-PhNCN})_2]$ (2)	15
5.2.3. Crystal structure of $[\text{Co}(\text{py}_2\text{C}(\text{OH})\text{O})(\text{py}_2\text{C}(\text{OCH}_2\text{CH}_3)\text{O})][\text{NO}_3] \cdot 3\text{H}_2\text{O}$ (3)	17
5.2.4. Crystal structure of $[\text{Zn}_2\text{Tb}(\mu_2\text{-py}_2\text{C}(\text{OCH}_2\text{CH}_3)\text{O})_3(\mu_3\text{-py}_2\text{C}(\text{OCH}_2\text{CH}_3)\text{O})(\text{NO}_3)(\text{H}_2\text{O})][\text{Tb}(\text{NO}_3)_5]$ (4)	18
5.2.5. Crystal structure of $[\text{Dy}_5\text{Co}_4(\text{py}_2\text{C}(\text{OH})\text{O})_4(\mu_3\text{-py}_2\text{CO}_2)_4(\mu_4\text{-py}_2\text{CO}_2)_2(\text{O})_2(\text{H}_2\text{O})_6(\text{NO}_3)_2][\text{NO}_3]_5$ (5)	19
5.3. Magnetic properties	21
5.3.1. Single molecule magnet behavior	27
6. EXPERIMENTAL SECTION	30
6.1. Materials and methods	30
6.2. Preparation of the R-Phenylcyanamides	30

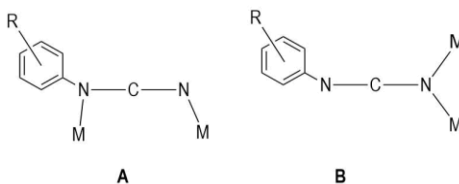
6.3. Preparation of the metal complexes	32
6.3.1 Preparation of $[\text{Co}_4(\mu_3\text{-py}_2\text{C}(\text{OH})\text{O})_4(4\text{-Br-CF}_3\text{-PhNCN})_2(\text{PhCOO})_2]$ (1)	32
6.3.2 Preparation of $[\text{Co}_4(\mu_2\text{-py}_2\text{C}(\text{OH})\text{O})_2(\mu_3\text{-py}_2\text{C}(\text{OCH}_3)\text{O})_2(\mu_2\text{-4-Cl-PhNCN})(4\text{-Cl-PhNCN})_2]$ (2)	32
6.3.3 Preparation of $[\text{Co}(\text{py}_2\text{C}(\text{OH})\text{O})(\text{py}_2\text{C}(\text{OCH}_2\text{CH}_3)\text{O})][\text{NO}_3]\cdot 3\text{H}_2\text{O}$ (3).	33
6.3.4 Preparation of $[\text{Zn}_2\text{Tb}(\mu_2\text{-py}_2\text{C}(\text{OCH}_2\text{CH}_3)\text{O})_3(\mu_3\text{-py}_2\text{C}(\text{OCH}_2\text{CH}_3)\text{O})(\text{NO}_3)(\text{H}_2\text{O})][\text{Tb}(\text{NO}_3)_5]$ (4)	33
6.3.5. Preparation of $[\text{Dy}_5\text{Co}_4(\text{py}_2\text{C}(\text{OH})\text{O})_4(\mu_3\text{-py}_2\text{CO}_2)_4(\mu_4\text{-py}_2\text{CO}_2)_2(\text{O})_2(\text{H}_2\text{O})_6(\text{NO}_3)_2][\text{NO}_3]_5$ (5)	34
7. CONCLUSIONS	34
8. REFERENCES AND NOTES	37
9. ACRONYMS	39
APPENDICES	41
Appendix 1: IR spectra	42
Appendix 2: Crystal data and selected bond lengths and angles.	45

1. SUMMARY

Five compounds have been synthesized in this work: $[\text{Co}_4(\mu_3\text{-py}_2\text{C}(\text{OH})\text{O})_4(4\text{-Br-3-CF}_3\text{-PhNCN})_2(\text{PhCOO})_2]$ (**1**), $[\text{Co}_4(\mu_2\text{-py}_2\text{C}(\text{OH})\text{O})_2(\mu_3\text{-py}_2\text{C}(\text{OCH}_3)\text{O})_2(\mu_2\text{-4-Cl-PhNCN})_2(4\text{-Cl-PhNCN})_2]$ (**2**), $[\text{Co}(\text{py}_2\text{C}(\text{OH})\text{O})(\text{py}_2\text{C}(\text{OCH}_2\text{CH}_3)\text{O})][\text{NO}_3] \cdot 3\text{H}_2\text{O}$ (**3**), $[\text{Zn}_2\text{Tb}(\mu_2\text{-py}_2\text{C}(\text{OCH}_2\text{CH}_3)\text{O})_3(\mu_3\text{-py}_2\text{C}(\text{OCH}_2\text{CH}_3)\text{O})(\text{NO}_3)(\text{H}_2\text{O})][\text{Tb}(\text{NO}_3)_5]$ (**4**) and $[\text{Dy}_5\text{Co}_4(\text{py}_2\text{C}(\text{OH})\text{O})_4(\mu_3\text{-py}_2\text{CO}_2)_4(\mu_4\text{-py}_2\text{CO}_2)_2(\text{O})_2(\text{H}_2\text{O})_6(\text{NO}_3)_2][\text{NO}_3]_5$ (**5**). The metal ions of the five compounds are connected through oxo-bridges from the Di(2-pyridil) ketone derivatives formed after solvolysis and a posterior deprotonation. In addition the Co(II) atoms of compound **2** are connected by two R-phenylcyanamides in the *end-on* coordination mode. The magnetic susceptibility measurements were performed for compounds **1**, **2**, **4** and **5**. Compound **1** and **2** exhibit a ferromagnetic coupling between the Co(II) metal ions. Compound **4** shows paramagnetic behaviour and **5** exhibit weak antiferromagnetic coupling between the Dy(II) ions. Compounds **1**, **2** and **5** show SMM (Single Molecular Magnet) behaviour. The relaxation time of magnetization hasn't been calculated.



Dpk derivatives after deprotonation: $\text{py}_2\text{C}(\text{OH})\text{O}^-$ (A), $\text{py}_2\text{C}(\text{OR})\text{O}^-$ (B) and $\text{py}_2\text{CO}_2^{2-}$ (C)

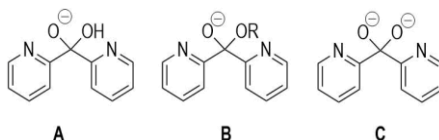


End-to-end(A) and *end-on*(B) coordination modes of R-phenylcyanamido ligands

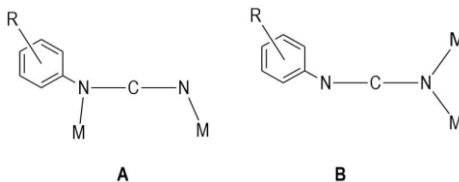
Keywords: Di(2-pyridil)ketone, R-phenylcyanamides, ferromagnetic coupling, lanthanides and SMM (single molecular magnets).

2. RESUM

En aquest treball de final de grau s'han sintetitzat cinc compostos diferents: : $[\text{Co}_4(\mu_3\text{-py}_2\text{C}(\text{OH})\text{O})_4(4\text{-Br-3-CF}_3\text{-PhNCN})_2(\text{PhCOO})_2]$ (**1**), $[\text{Co}_4(\mu_2\text{-py}_2\text{C}(\text{OH})\text{O})_2(\mu_3\text{-py}_2\text{C}(\text{OCH}_3)\text{O})_2(\mu_2\text{-4-Cl-PhNCN})_2(4\text{-Cl-PhNCN})_2]$ (**2**), $[\text{Co}(\text{py}_2\text{C}(\text{OH})\text{O})(\text{py}_2\text{C}(\text{OCH}_2\text{CH}_3)\text{O})][\text{NO}_3] \cdot 3\text{H}_2\text{O}$ (**3**), $[\text{Zn}_2\text{Tb}(\mu_2\text{-py}_2\text{C}(\text{OCH}_2\text{CH}_3)\text{O})_3(\mu_3\text{-py}_2\text{C}(\text{OCH}_2\text{CH}_3)\text{O})(\text{NO}_3)(\text{H}_2\text{O})][\text{Tb}(\text{NO}_3)_5]$ (**4**) i $[\text{Dy}_5\text{Co}_4(\text{py}_2\text{C}(\text{OH})\text{O})_4(\mu_3\text{-py}_2\text{CO}_2)_4(\mu_4\text{-py}_2\text{CO}_2)_2(\text{O})_2(\text{H}_2\text{O})_6(\text{NO}_3)_2][\text{NO}_3]_5$ (**5**). Els ions metàl·lics dels sis compostos estan connectats entre si per l'àtom d'oxigen del derivats formats a partir de la Di(2-pyridil)cetona i una posterior desprotonació d'aquests. Els ions Co(II) del compost **2** també estan connectats mitjançant dos R-fenilcianamides en el mode de coordinació *end-on*. S'han realitzat les mesures de la susceptibilitat magnètica per els compostos **1**, **2**, **4** i **5**. Els compostos **1** i **2** presenten comportament ferromagnètic. El compost **4** és paramagnètic el **5** presenta acoblament antiferromagnètic feble entre els àtoms de Dy(II). Els compostos **1**, **2** i **5** presenten comportament SMM (*Single Molecular Magnet*). No s'ha calculat el temps de relaxació de la magnetització.



Derivats de la dpk després de desprotonació: $\text{py}_2\text{C}(\text{OH})\text{O}^-$ (A), $\text{py}_2\text{C}(\text{OR})\text{O}^-$ (B) and $\text{py}_2\text{CO}_2^{2-}$ (C)



End-to-end(A) and *end-on*(B) modes de coordinació dels lligands R-fenilcianamida

Paraules clau: Di(2-pyridil)cetona, R-fenilcianamides, acoblament ferromagnètic, lantànids i SMM(single molecular magnets).

3. INTRODUCTION

3.1. DI(2-PYRIDIL) KETONE CHEMISTRY.

Di-pyridil ketone (dpk) Fig. 1A is an interesting organic ligand in 3*d*-metal cluster chemistry and most of its interest resides in the carbonyl group. It can act as a neutral ligand since it has three potential donor groups: two N atoms from the pyridil rings and an O atom from the carbonyl group. This compound improves its coordination chemistry when its derivatives are formed after hydration: the mechanism consists of a nucleophilic attack of a H₂O molecule to the C atom of the carbonyl group in a basic medium.[1] The derivative formed after hydration is the gem-diol (py₂C(OH)₂) Fig. 1B. Also a similar reaction can take place if the nucleophilic agent is an alcohol molecule such as methanol or ethanol Fig. 1D and E. Then the hemiacetal (py₂C(OR)(OH)) Fig. 1C derivative is formed. The hydrated or hemiacetal form is favoured when the O atom from the carbonyl group coordinates to a metal ion. This fact increases the electrophilic character of the carbonyl C atom.

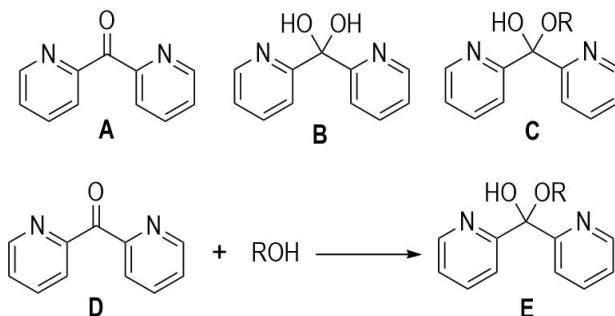


Fig. 1. dpk (A), gem-diol derivative (B) hemiacetal derivative (C). (D) and (E) represents the hydration reaction where R = -H, -CH₃ or -CH₂CH₃.

The gem-diol and the hemiacetal derivatives of dpk in its neutral form can coordinate to the metal ion by the N atoms from the pyridil ring and by the O atom but the M-O bond usually turns out to be weak. The coordination modes of this species increase when they get deprotonated. Then the py₂C(OH)O⁻ Fig. 2A, py₂C(OR)O⁻ Fig. 2B and py₂CO₂²⁻ Fig. 2C monoanion and dianion respectively will be formed.[1] These anions show a great coordinative flexibility since the negatively charged O atoms are capable to bridge two or three metal ions in the py₂C(OH)O⁻ and py₂C(OR)O⁻ derivatives and until five metal ions in the py₂CO₂²⁻ derivative.[2]

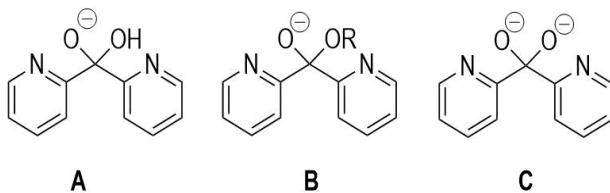


Fig.2. Dpk derivatives after deprotonation: $\text{py}_2\text{C}(\text{OH})\text{O}^-$ (A), $\text{py}_2\text{C}(\text{OR})\text{O}^-$ (B) and $\text{py}_2\text{CO}_2^{2-}$ (C)

Some of the coordination modes that had been found in previous studies of these anions [2] are shown in Fig. 3

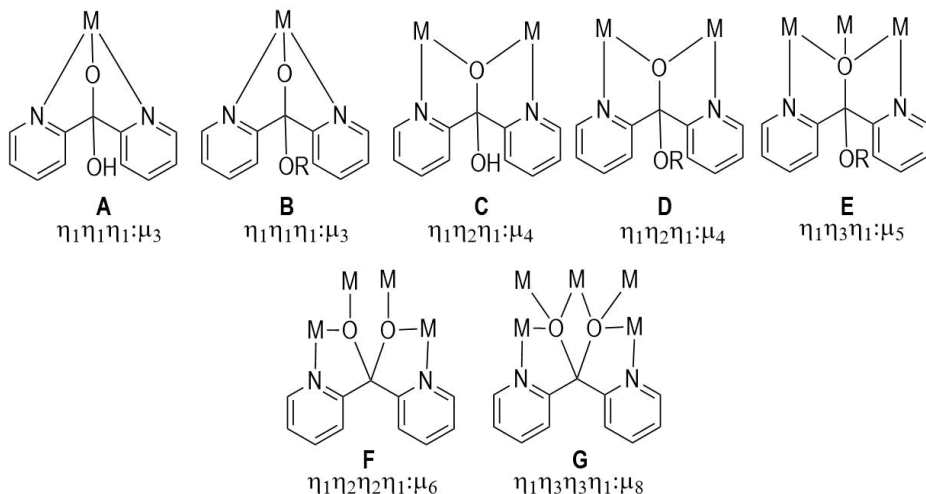


Fig.3. Different coordination modes of $\text{py}_2\text{C}(\text{OH})\text{O}^-$ (A) and (C), $\text{py}_2\text{C}(\text{OR})\text{O}^-$ (B), (D) and (E) and $\text{py}_2\text{CO}_2^{2-}$ (F) and (G).

3.2. R-PHENYLCYANAMIDES CHEMISTRY.

R-phenylcyanamides (R-PhHNCN) are interesting compounds acting as bridging ligands in complexes with a large S ground state values such as Co(II). The amine H atom is quite acid due to the stability, because of the different resonant forms, of the respective anion. Therefore the R-PhNCN coordinates in the anionic form and it presents two coordination modes: *end-to-end* Fig.4A and *end-on* Fig4B. The *end-on* coordination mode leads to ferromagnetic coupling in a large range of M-N-M angles (where M is the metal ion) when the N atom is doubly bridged to the M atoms in the axial-equatorial positions of the metal.[3] A similar behaviour has been demonstrated for other bridging ligands such as azido or cyanate. [4], [5]

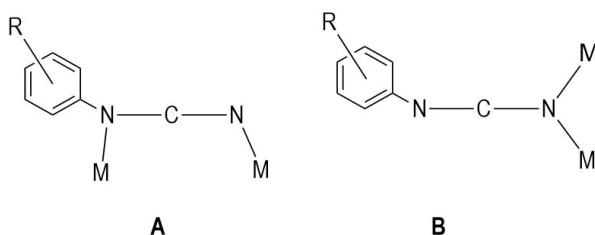


Fig.4. End-to-end(A) and end-on(B) coordination modes of R-phenylcyanamido ligands.

3.3. MAGNETISM

In an M-X-M system (M refers to a metal ion and X to a diamagnetic bridging ligand) there are three group orbitals which their lineal combination gives three molecular orbitals (MOs). One is a bonding orbital, the most stable one, which is fully occupied, another one is a high energy antibonding orbital and lastly a non-bonding orbital. If two electrons are occupying one MO the final ground state is a spin singlet ($S_T=0$) and the resulting interaction is called antiferromagnetic. If the electrons are occupying different MO the ground state will be a spin triplet ($S_T=1$) and the final interaction is called ferromagnetic. The electrostatic interaction between the electrons of two atoms is represented by the Heisenberg-Dirac-Van Vleck (HDVV) Hamiltonian Eq.1.[6]

$$\hat{H} = -J_{ij} \hat{S}_i \hat{S}_j \quad (1)$$

Where \hat{S}_i and \hat{S}_j are the spins of the paramagnetic ions i and j . The J_{ij} factor corresponds to the exchange constant between the S_i and S_j spins [6]. J is the energy gap between the spin singlet-triplet ground state and if $J > 0$ the interaction corresponds to a ferromagnetic coupling and if $J < 0$ the interaction is antiferromagnetic.[7]

The interaction energy between different paramagnetic ions can be calculated with the HDVV Hamiltonian but for polynuclear compounds it becomes more difficult to calculate the energies due to the complexity of the system. Also it is important to study the magnetic exchange in a more microscopic way according to the Kahn and the Hoffmann models in order to relate the magnetic behaviour with the structure of the compound.[6]

The magnetic exchange parameter J is decomposed into two components Eq.2[6]: one ferromagnetic that provides a parallel alignment of the spins and one antiferromagnetic that provides an antiparallel alignment of the spins.[7]

$$J = J_F + J_{AF} \quad (2)$$

Where $J_{AF} \propto -\sum \Delta^2$ and $J_F \propto k$. ($J_F > 0$ and $J_{AF} < 0$)

The antiferromagnetic component (J_{AF}) is proportional to Δ^2 , the square of the energy gap between the corresponding MOs (magnetic orbitals) constructed from the three group orbitals.

The ferromagnetic component (J_F) is proportional to k Eq.3 [6] which is the two-electron exchange integral between the two magnetic orbitals.

$$k = \langle a(1)b(2) | e^2/r_{12} | a(2)b(1) \rangle \quad (3)$$

Where a and b are the magnetic orbitals that are single occupied by electrons from centres (1) and (2) and e^2/r_{12} is the electrostatic interaction between the electrons 1 and 2. Eq. 3 describes the coupling interaction between electrons from centre (1) and (2) and is based on the orthogonality of the magnetic orbitals. Both Kahn's and Hoffmann's models predict that orthogonal orbitals lead to ferromagnetic behaviour and non-orthogonal orbitals lead to antiferromagnetic behaviour.[7] For instance, in compounds with metal ions bridged by the O atom from the dpk derivatives after solvolysis and a posterior deprotonation, a ferromagnetic behaviour predominates when the M-O-M angles are close to 95° . [2], [5], [6] Also R-phenylcyanamides bridged to the metal ions in the *end-on* coordination mode with N-M-N angles close to 100° lead to ferromagnetic coupling.[8]

In addition the two-electron exchange integral k can be written as Eq.4 where ρ_i is the overlap density at the point i and $r(12)$ is the interelectronic distance between centres (1) and (2). This expression indicates that k , therefore J_F , depends on the overlap density in the space that corresponds to the bridging zone. Also k is inversely proportional to $r(12)$ so the smallest the distance between the metal ions, the larger the J_F component will be and so will be the ferromagnetic interaction. In most cases the two components exist and when the J_{AF} is almost negligible the global interaction is ferromagnetic.[6]

$$k = \int \rho_i(1)\rho_i(2) / r(12) dV_1 dV_2 \quad (4)$$

The J value can be calculated using computational methods or by fitting the magnetic data obtained experimentally. Also is interesting to study how the coupling parameters are modified when distances, angles and other parameters, for example the use of different bridging ligands, vary in a series of related complexes.

3.3.1. Lanthanides magnetic properties.

Magnetic properties of trivalent rare earth ions are quite different from transition metal ions due to the large spin-orbit coupling that lanthanides present. For a $4f^n$ electron configuration the degenerated ground states are split into ^{2S+1}L spectroscopic terms due to the interelectronic repulsion. In the ^{2S+1}L spectroscopic term L is the total orbital angular momentum, $2S+1$ is the spin multiplicity and S is the total spin angular momentum. The interelectronic repulsion is large because the wave functions of the $4f$ electrons are contracted. The ^{2S+1}L term are split into J states due to the spin orbit coupling giving $^{2S+1}L_J$ spectroscopic terms where J is the total angular momentum number. The J value in the ground state is $J= L-S$ if the f shell is half filled (f^1-f^6) and $J=L+S$ if the f shell is more than half filled (f^7-f^{14}) and the ^{2S+1}L are split on as many states as $|L-S| \leq J \leq L+S$ can give. Finally the ligand-field effect caused by the ligands that are surrounding the lanthanide ion affect the magnetic properties of these complexes by inducing large magnetic anisotropies. Consequently the spectroscopic levels are split into Stark sublevels. The latter perturbation is much smaller than the interelectronic repulsion and the spin-orbit coupling because the $4f$ orbitals are more shielded by the $5d^1, 6s^2$ therefore the ligand-field effect will be lower than for a d metal ion.

At room temperature only the Stark sublevels are populated then the lanthanide compound will follow the Curie Law. At low temperatures there is a depopulation of these sublevels that produces a deviation of the χ_M vs. T values. (χ_M stands for the molar magnetic susceptibility).

The unpaired electrons disposed into the $4f^n$ orbitals are highly contracted and energetically protected by the $5s$ and $5p$ orbitals that are totally occupied so the interaction between $4f^n-4f^n$ is usually weak. Thus, the antiferromagnetic or ferromagnetic coupling between Ln-Ln atoms is small with a slight coupling constant of 1 cm^{-1} or even less.[7], [9], [10],

3.3.2. Single-Molecule Magnets.

A single-molecule magnet (SMM) is an isolated molecule system that below a certain temperature is able to keep the magnetization temporarily, it shows a slow relaxation of the magnetization, after applying an external field.[6]

After applying an external field the magnetic moment aligns into one of the two possible directions: α or β (up-spin state or down-spin state). These two states are separated by an effective energy barrier U_{eff} . [11] The U_{eff} maximum value is $-DS^2$ for integer spin and $-D(S^2 - 1/2)$ for half integer spin values where S is the total spin number and D is the zero-field splitting parameter. [1] The larger U_{eff} value the slower the relaxation magnetization therefore the system will return to thermal equilibrium in a longer range of time. Thus an SMM requires a large S value in the ground state and a strong magnetic anisotropy which is represented by the D parameter. [2], [6]

Compounds with trivalent lanthanides ions are good SMM since they own large single-ion anisotropy and a large magnetic moment in the ground state. [10], [12]

In order to detect experimentally the SMM behaviour of the obtained compounds we have measured, under alternating current (ac) conditions, the in-phase (χ_M') and out-of-phase (χ_M'') components of the magnetic susceptibility and studied the dependence of this components with the frequency and temperature. SMM compounds show dependence of the χ_M' and χ_M'' components with frequency and temperature.

The relaxation time of the magnetization can be calculated by the Arrhenius equation Eq.5 where τ_0^{-1} is the relaxation time of magnetization at infinite temperatures, U_{eff} is the effective anisotropic barrier and k_B is the Boltzmann constant.[10], [11]

$$\tau_0 = \tau_0^{-1} \exp\left(\frac{-U_{eff}}{k_B T}\right) \quad (5)$$

4. OBJECTIVES

The objectives of this work are:

- i. The synthesis and characterization of two R-phenylcyanamide ligands: 4-chlorophenylcyanamide (4Cl-PhNCN) and 4-chloro-3-trifluorophenylcyanamide (4Cl-3CF₃-PhNCN).
- ii. The synthesis of metallic compounds with R-phenylcyanamides, dpk, 1,10-phenantroline and carboxylates as ligands using Ln(III), Co(II) and Zn(II) as metal ions and the posterior characterization with elemental analysis, infrared spectroscopy and X-ray diffraction.
- iii. The study of the magnetic properties of the metallic compounds obtained and their SMM behaviour with the objective, if it is possible, to get a relation between the magnetic behaviour with the structure of the compound.

5. RESULTS AND DISCUSSION.

5.1. IR SPECTROSCOPY.

A summary of the most important IR absorption bands corresponding to the two R-phenylcyanamide ligands is given in Table 1.[3]

4-ClPhHNCN (L1)	3155-2876 m	2237 s	1602 m	1499 s
4-Cl-3CF₃-PhHNCN (L2)	3162-2907 m	2243 s	1619 m	1486 s

Table 1. IR absorption bands (cm⁻¹) of compounds **L1** and **L2** 'm' and 's' stand for the intensity of the bands: 'm' for medium and 's' for strong signal.

The absorption bands are assigned for compounds $[\text{Co}_4(\mu_3\text{-py}_2\text{COOH})_4(4\text{-Br-3-CF}_3\text{-PhNCN})_2(\text{PhCOO})_2]$ (**1**), $[\text{Co}_4(\mu_2\text{-py}_2\text{COOH})_2(\mu_3\text{-py}_2\text{COOCH}_3)_2(\mu_2\text{-4-Cl-PhNCN})_2(4\text{-Cl-PhNCN})_2]$ (**2**), $[\text{Co}(\text{py}_2\text{C}(\text{OH})\text{O})(\text{py}_2\text{C}(\text{CH}_2\text{CH}_3)\text{O})][\text{NO}_3]\cdot 3\text{H}_2\text{O}$ (**3**), $[\text{Zn}_2\text{Tb}(\mu_2\text{-py}_2\text{C}(\text{OCH}_2\text{CH}_3)\text{O})_3(\mu_3\text{-py}_2\text{CO}(\text{CH}_2\text{CH}_3)\text{O})(\text{NO}_3)(\text{H}_2\text{O})][\text{Tb}(\text{NO}_3)_5]$ (**4**) and $[\text{Dy}_5\text{Co}_4(\text{py}_2\text{C}(\text{OH})\text{O})_4(\mu_3\text{-py}_2\text{CO}_2)_4(\mu_4\text{-py}_2\text{CO}_2)_2(\text{O})_2(\text{H}_2\text{O})_6(\text{NO}_3)_2][\text{NO}_3]_5$ (**5**) in Table 2. [3], [4], [8], [13]

	R-PhHNCN, $\nu_{(C\equiv N)}$	Dpk, $\nu_{(C-O)}$	Pyridil stretching	Pyridil breathing	Pyridil C-H out of plane
1	2138, 2069	1590	1477	1059	767
2	2120 split	1584	1486	1062	773
3	-	1606	1438	1014	767
4	-	1600	1479	1049	773
5	-	1606	1442	1014	767

Table 2. Selected absorption bands [cm^{-1}] from IR spectra of compounds **1** to **5**

5.2. CRYSTAL STRUCTURES.

5.2.1. Crystal structure of compound $[\text{Co}_4(\mu_3\text{-py}_2\text{C}(\text{OH})\text{O})_4(4\text{-Br-3-CF}_3\text{-PhNCN})_2(\text{PhCOO})_2]$ (**1**)

The compound obtained consists of a tetranuclear molecule where the central metal core is in the form of a cube where the four Co(II) are occupying opposite corners. The structure of compound **1** is shown in Fig 5. and the selected bond lengths are listed in Table 3(Apx.2). The other vertexes are occupied by O atoms from the dpk derivative after solvolysis. The four Co(II) are octahedrally coordinated and they are bridged by four O atoms from the gem-diol form of dpk. The O(1), O(3), O(5) and O(7) atoms from the $\text{py}_2\text{C}(\text{OH})\text{O}^-$ anion are triply bridging (μ_3) the Co(II) metal ions with distances in the range of 2.0210-2.2583 Å. The Co-O-Co angles (the O atom comes from the gem-diol derivative) range from 95.06° to 105.25° where the Co(1)-O(1)-Co(3) angle is 96.83°, the Co(3)-O(3)-Co(4) angle is 95.79°, the Co(4)-O(5)-Co(4) angle is 99,11° and the Co(1)-O(7)-Co(2) angle is 95.06°. As terminal ligands there are two 4-Br-3-CF₃-PhNCN anions that bridge by the nitrile nitrogen. The Co(1)-N(1) distance is 2.0170 Å and the Co(3)-N(3) distance is 2.0260 Å. Also there are two benzoate anions as terminal ligands. The

latter ligand probably comes from an impurity of the R-PhNCN synthesis since benzoate is an intermediate in the reaction mechanism Fig.25G(Experimental section). The Co(4)-O(9) distance is 2.0486 Å and the Co(2)-O(11) distance is 2.0528 Å. The Co(1), Co(2), Co(3) and Co(4) octahedral coordination is completed by two N atoms each, N(5) and N(8), N(10) and N(11), N(6) and N(7), N(9) and N(12) respectively, from the pyridil rings of the (py)₂C(OH)O⁻ anion. The Co---Co intermetallic distances are in the range of 3.189-1.314 Å.

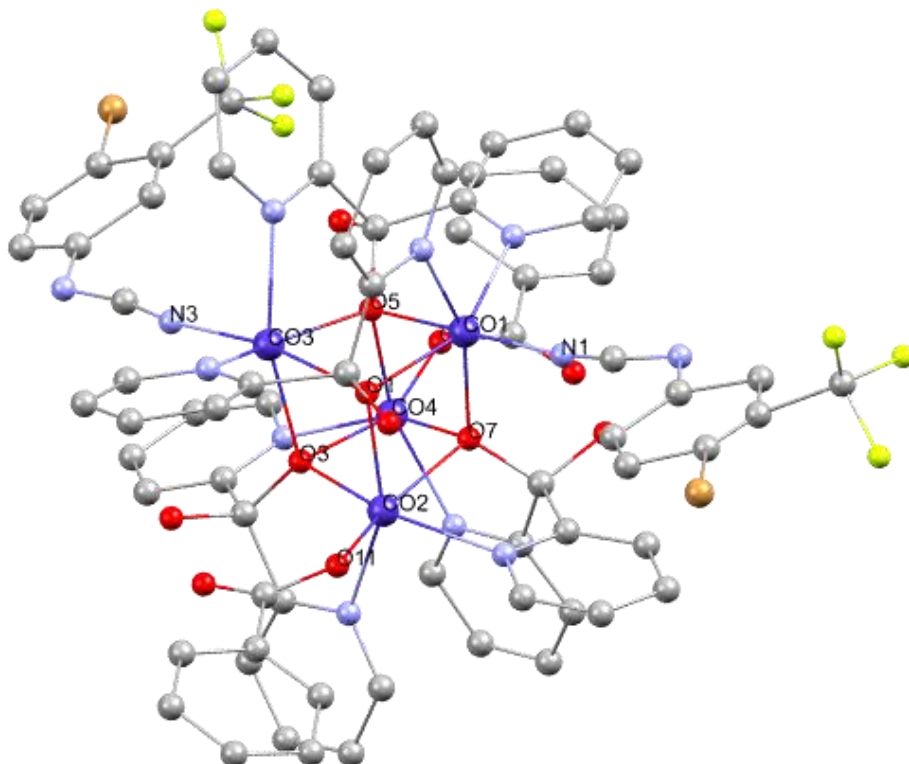


Fig.5. Partially labelled structure of (1) Colour code: dark blue = Co, red = O, light blue = N, grey = C, brown = Br, yellow = F

5.2.2. Crystal structure of compound [Co₄(μ₂-py₂C(OH)O)₂(μ₃-py₂C(OCH₃)O)₂(μ₂-4-Cl-PhNCN)₂(4-Cl-PhNCN)₂] (2)

The compound obtained consists in a centrosymmetric tetranuclear molecule with a defective double cubane metal core. A defective double cubane is a structure where two cubanes are sharing one face and each cubane has one missing vertex.[2] The structure of

compound **2** is shown in Fig.6 and selected bond lengths are listed in Table 4(Apx.2). The four Co(II) metal ions are located at four corners of the metal core structure and they are bridged by two N atoms from the 4-Cl-PhNCN ligand and four O atoms from the dpk derivatives after solvolysis. The two 4Cl-PhNCN acting as bridging ligands are in the *end-on* coordination mode. The Co(2)-N(9), Co(1)-N(9), Co(4)-N(13) and Co(3)-N(13) distances are 2.169, 2.094, 2.117 and 2.098 Å respectively and the Co(1)-N(9)-Co(2) and Co(4)-N(13)-Co(3) angles are 101.89° and 101.52° respectively. There are four dpk derivatives in the structure of this compound. Two come from the hemiacetal derivative and two come from the gem-diol derivative of dpk. The O(1) and O(7) atoms from the py₂C(OH)O⁻ anion bridge to the Co(1) with Co(4) and Co(2) with Co(3) respectively with Co-O distances in the range of 2.036-2.164 Å. The Co(1)-O(1)-Co(4) angle is 99.41° and the Co(2)-O(7)-Co(3) angle is 98.48°. The O(3) and O(5) atoms from the py₂C(OH)O⁻ anion bridge Co(1), Co(3) and Co(4) and Co(1), Co(2) and Co(3) metal ions respectively with Co-O distances in the range of 2.028-2.2261 Å. The Co(2)-O(5)-Co(3) angle is 95.89° and the Co(3)-O(3)-Co(4) angle is 96.95°. The four Co(II) atoms are hexacoordinated. The octahedral coordination of the Co(1), Co(2), Co(3) and Co(4) atoms is completed by the N(1) and N(1), N(5) and N(7), N(6) and N(8), N(2) and N(4) atoms from the pyridil ring of the dpk derivatives. In addition the Co(2) and Co(4) metal ions octahedral coordination is completed by the N(11) and N(15) atoms respectively from the 4-Cl-PhNCN anion that acts as a monodentate ligand. The Co(2)-N(11) and Co(4)-N(15) bond lengths are 2.015 and 2.043 Å. The Co---Co intermetallic distances are in the range of 3.160-3.311Å.

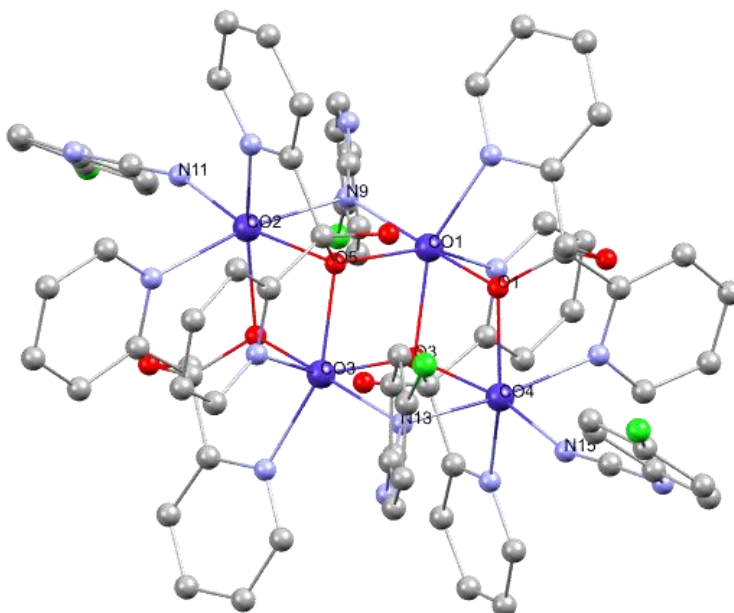


Fig. 6. Partially labelled structure of **(2)** Colour code: dark blue = Co, red = O, light blue = N, grey = C, green = Cl

5.2.3. Crystal structure of compound $[\text{Co}(\text{py}_2\text{C}(\text{OH})\text{O})(\text{py}_2\text{C}(\text{OCH}_2\text{CH}_3)\text{O})][\text{NO}_3] \cdot 3\text{H}_2\text{O}$ (**3**)

The compound obtained consists in a mononuclear molecule where the Co(II) has oxidized along the reaction process to Co(III). The structure of compound **3** is shown in Fig.7 and selected bond lengths are listed in Table 5(Apx.2) The Co(III) has an octahedral coordination sphere. Two different type of the dpk derivatives are bonded to the metal ion: one is in the gem-diol form ($\text{py}_2\text{C}(\text{OH})\text{O}^-$) and the other is in the hemiacetal form ($\text{py}_2\text{C}(\text{OCH}_2\text{CH}_3)\text{O}^-$). The O(4) atom from the $\text{py}_2\text{C}(\text{OH})\text{O}^-$ anion is bonded to the metal ion with a Co(1)-O(4) distance of 1.8848 Å. The N(3) and N(4) atoms from the pyridil rings are bonded to the metal ion with Co(1)-N(3) and Co(1)-N(4) distances of 1.9378 and 1.9132 Å respectively. The O(1) atom from the $\text{py}_2\text{C}(\text{OCH}_2\text{CH}_3)\text{O}^-$ anion is bonded to the metal ion with a Co(1)-O(1) distance of 1.8931 Å. The N(1) and N(2) atoms from the pyridil rings are bridged to the metal ion with Co(1)-N(1) and Co(1)-N(2) distances of 1.9360 and 1.9158 Å respectively. There is a nitrate anion as counterion and three H_2O molecules in the crystal structure.

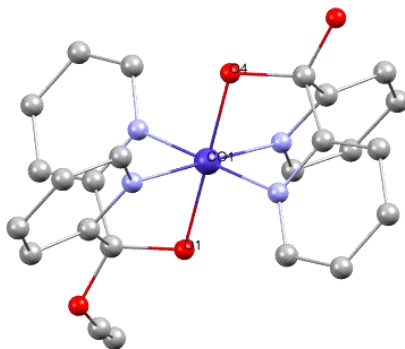


Fig.7. Partially labelled structure of (3) Colour code: dark blue = Co, red = O, light blue = N, grey = C.

5.2.4. Crystal structure of compound $[\text{Zn}_2\text{Tb}(\mu_2\text{-py}_2\text{C}(\text{OCH}_2\text{CH}_3)\text{O})_3(\mu_3\text{-py}_2\text{C}(\text{OCH}_2\text{CH}_3)\text{O})(\text{NO}_3)(\text{H}_2\text{O})][\text{Tb}(\text{NO}_3)_3]$ (4)

The compound obtained consists of a trinuclear molecule with a triangle metal core. The structure of compound 4 is shown in Fig.8 and selected bond lengths are listed in Table 6(Apx.2). The metal ions of the compound are two Zn(II) metal ions and one Tb(III) metal ion and they are located at three corners of the triangle. The metal ions are bridged by four O atoms from the dpk derivative after solvolysis. The four dpk derivatives are in the hemiacetal form ($\text{py}_2\text{C}(\text{OCH}_2\text{CH}_3)\text{O}^-$) but the O atoms bridge the metal ions differently. The O(1), O(3) and O(5) atoms from the $\text{py}_2\text{C}(\text{OCH}_2\text{CH}_3)\text{O}^-$ anion are doubly bridging the metal ions with Zn-O distances in the range of 2.0163-2.0703 Å and Tb-O bond distances are 2.2732 and 2.2663 Å. The Tb(1)-O(1)-Zn(1), Tb(1)-O(3)-Zn(2) and Zn(1)-O(5)-Zn(2) angles are 109.61°, 107.64°, 106.73° respectively. The O(7) atom from the $\text{py}_2\text{C}(\text{OCH}_2\text{CH}_3)\text{O}^-$ anion is triply bridging the metal ions with Zn-O(7) distances of 2.1897 and 2.4413 Å and Tb-O(7) distance of 2.3449 Å. The Tb(1)-O(7)-Zn(1), Tb(1)-O(7)-Zn(2) and Zn(1)-O(7)-Zn(2) angles are 101.73°, 93.93° and 90.00° respectively.

Both Zn(II) metal ions are hexacoordinated. The octahedral coordination of Zn(1) and Zn(2) is completed by the N(5), N(7) and N(4), N(6) atoms respectively from the pyridil ring of the dpk derivatives. The Tb(III) metal ion is octacoordinated and its coordination sphere is completed by two N(1) and N(3) atoms from the pyridil ring of the dpk derivatives, a O(12) atom from a H_2O molecule and two O atoms, O(9) and O(10), from a NO_3^- anion. The Zn(1)---Zn(2), Zn(1)---Tb(1)

and Zn(2)---Tb(1) intermetallic distances are 3.280, 3.520 and 3.499 Å respectively and the Tb(1)---Tb(2) intermetallic distance is 10.362 Å. There is a $\text{Tb}(\text{NO}_3)_5^{2-}$ as a conterion.

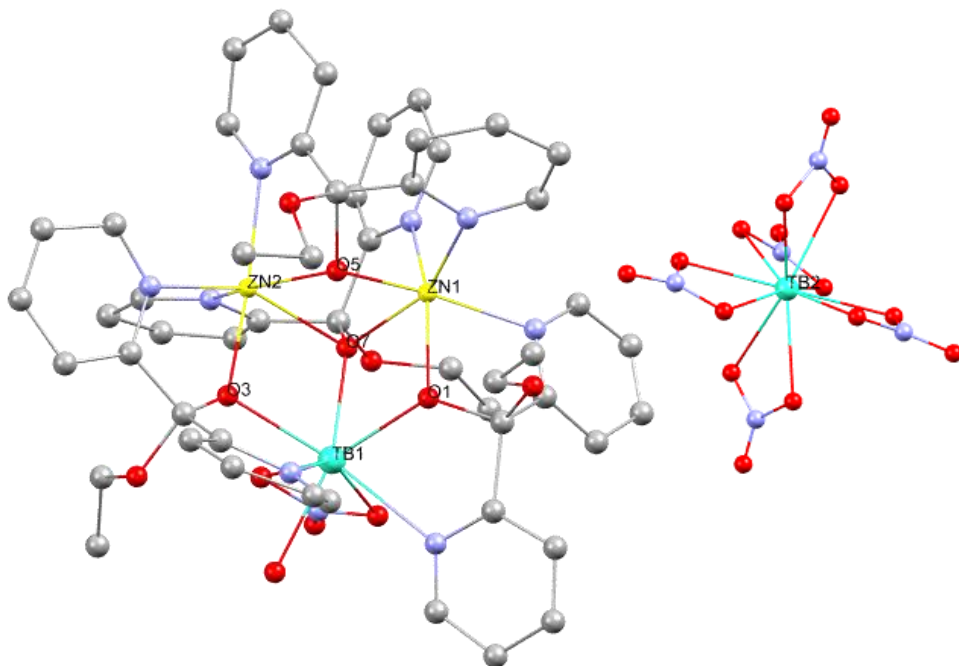


Fig.8. Partially labelled structure of (4). Colour code: turquoise = Tb, yellow = Zn, red = O, light blue = N, grey = C

6.2.5. $[\text{Dy}_5\text{Co}_4(\text{py}_2\text{C}(\text{OH})\text{O})_4(\mu_3\text{-py}_2\text{CO}_2)_4(\mu_4\text{-py}_2\text{CO}_2)_2(\text{O})_2(\text{H}_2\text{O})_6(\text{NO}_3)_2][\text{NO}_3]_5$ (5)

The compound obtained presents a symmetry centre therefore only the metal atoms contained in one asymmetric unit and its respective coordination sphere will be described. Each asymmetric unit consists of a $\text{Co}^{\text{III}}\text{Dy}^{\text{III}}$ core where the Co(II) used in the synthesis has oxidized along the reaction process to Co(III). The structure of compound 5 is shown in Fig.9 and selected bond lengths are listed in Table 7(Apx.2).

Co(1) and Co(2) of each asymmetric unit are hexacoordinated. The O(7) and O(1) atoms from a dpk derivative after solvolysis in the gem-diol form ($\text{py}_2\text{C}(\text{OH})\text{O}^-$) are singly bonded to the Co(1) and Co(2) metal ions respectively with Co-O distances of 1.893 and 1.888 Å. The N(6),

N(7) and N(1), N(2) atoms from the pyridil rings of the $\text{py}_2\text{C}(\text{OH})\text{O}^-$ anions are linked to Co(1) and Co(2) respectively with Co-N distances in the range of 1.913-1.946 Å.

There are two dpk derivatives that are in the $\text{py}_2\text{CO}_2^{2-}$ form in the $\eta^1:\eta^2:\eta^2:\eta^1:\mu_3$ coordination mode that are bonded to the Co(1) and Co(2) by the deprotonated O(5) and O(3) atoms respectively with Co-O distances in the range of 1.870-1.893 Å. The N(5), N(6) and N(3), N(4) from the pyridil rings of these $\text{py}_2\text{CO}_2^{2-}$ anions are bonded to Co(1) and Co(2) respectively with N-Co distances in the range of 1.921-1.946 Å. Each O atom from the $\text{py}_2\text{CO}_2^{2-}$ ligand is doubly bonded. For one of the $\text{py}_2\text{CO}_2^{2-}$ anion the O(5) atom is doubly bridged to the Co(1) and Dy(1) metal ions and the O(6) atom is doubly bridged to the Dy(1) and Dy(2) metal ions. For the other $\text{py}_2\text{CO}_2^{2-}$ anion the O(3) atom is doubly bridged to the Co(2) and Dy(3) metal ions and the O(4) atom is doubly bridged to the Dy(1) and Dy(3) metal ions. The Dy-O bond distances are in the range of 2.212-2.482 Å. The Co(1)-O(5)-Dy(1) and Co(2)-O(3)-Dy_a(3) angles are 152.9° and 155.8° respectively. The Dy(1)-O(6)-Dy(2) and Dy(1)-O(4)-Dy_a(3) angles are 94.16° and 97.2°. The symmetry transformations used to generate equivalent atoms is ($_a$) 1/2-x, 1/2-y, z

The three Dy(III) atoms are connected by the O(20) atom from an oxo bridge with Dy-O distances in the range of 2.377-2.398 Å. The Dy_a(1)-O(20)-Dy(2), Dy_a(1)-O(20)-Dy(3) and Dy(2)-O(20)-Dy(3) angles are 94.68°, 95.3° and 94.6° respectively.

A dpk derivative in the $\text{py}_2\text{CO}_2^{2-}$ form with a $\eta^1:\eta^3:\eta^2:\eta^1:\mu_4$ coordination mode is coordinated to the Dy(III) metal atoms. The O(9) atom is triply bridged to Dy(1), Dy(2) and Dy(3) metal ions with Dy-O bond distances in the range of 2.324-2.397 Å. The Dy_a(1)-O(9)-Dy(2), Dy_a(1)-O(9)-Dy(3) and Dy(2)-O(9)-Dy(3) angles are 98.00°, 96.6°, 96.20°. The O(19) atom is doubly bonded to Dy(2) and Dy(3) metal ions with Dy-O bond distances of 2.229 and 2.429 Å. The Dy(2)-O(19)-Dy(3) angle is 98.0°. The N(9) and N(10) atoms from the pyridil rings are bonded to the Dy(3) and Dy(1) metal ions respectively with bond distances of 2.557 and 2.570 Å.

The sphere coordination of Dy(1) is completed by the N(10) atom from the pyridil ring of the $\text{py}_2\text{CO}_2^{2-}$ dpk derivative and the O(14) and O(15) atoms from two H_2O molecules and the Dy(3) sphere coordination is completed by the O(13) atom from a H_2O molecule and the O(10) and O(11) atoms from a NO_3^- anion. There is a nitrate molecule as a conterion.

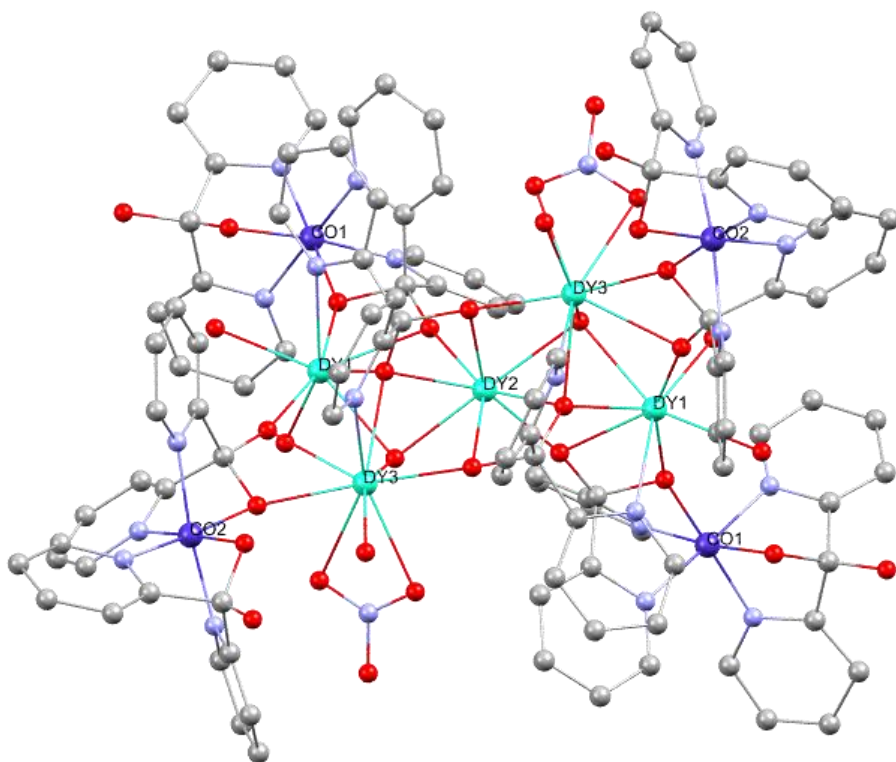


Fig.9. Partially labelled structure of (5). Color code: turquoise = Dy, dark blue = Co, light blue = N, red = O and grey = C.

5.3. MAGNETIC PROPERTIES.

Susceptibility and magnetization measurements were performed for compounds **1**, **2**, **4** and **5**. Compound **3** is a mononuclear Co(III) molecule therefore will be diamagnetic.

The $\chi_M T$ vs. T plot of compound **1** and **2** in the 300-2K range is shown in Fig.10 and Fig.11 respectively. Both compounds exhibit a similar behaviour. The $\chi_M T$ values increase gradually on cooling from $9.8 \text{ cm}^3 \text{ K mol}^{-1}$ for compounds **1** and from $12.9 \text{ cm}^3 \text{ K mol}^{-1}$ for **2** at 300K to a

maximum of $19.0 \text{ cm}^3 \text{ K mol}^{-1}$ for **1** and $18.3 \text{ cm}^3 \text{ K mol}^{-1}$ for **2** at 8 K and then decreases to $14.6 \text{ cm}^3 \text{ K mol}^{-1}$ for **1** and $13.9 \text{ cm}^3 \text{ K mol}^{-1}$ for **2** at 2K. This sudden decrease of $\chi_M T$ at low temperatures could be attributed to spin-orbit coupling and/or the presence of intermolecular interactions.[5], [8] For both compounds the $\chi_M T$ values at room temperature are larger than the one expected for four isolated Co(II) which is $7.48 \text{ cm}^3 \text{ K mol}^{-1}$ because of the orbital momentum contribution at high temperatures.[5] The $\chi_M T$ vs. T values obtained for compound **1** and **2** are to other Co_4 clusters found in the literature.[4], [5], [8], [13], [14]

The field dependence of magnetization of each compound was recorded at 2 K as shown in Fig.12 for **1** and Fig.13 for **2**. On increasing the external field, M values increase to $7.4 \text{ N}\mu\text{B}$ for compound **1** and to $8.1 \text{ N}\mu\text{B}$ for **2** at 5.02 T .

Saturation magnetization indicates that all electrons are aligned parallel to the magnetic field. [6] In this case, at the maximum external field applied at 2 K, compounds **1** and **2** don't arrive to the saturation point. The magnetization saturation point expected for a tetranuclear ferromagnetic Co(II) complex should be $\approx 12 \text{ N}\mu\text{B}$. [5] Saturation magnetization value (magnetization in the limit of low temperature and strong field applied) can be calculated as shown in Eq.5.[6]

$$\frac{M}{N_A \mu_B} = gS = g \frac{n}{2} \quad (5).$$

Where g is the spin g -factor ($g = 2.002319$ for a free electron), S is the total spin value of the sample that can be represented as $S = n/2$ where n is the number of unpaired electrons in the sample. [6] We could reach the saturation magnetization point of compounds **1** and **2** by applying a higher magnetic field than 5 T .

This behaviour indicates ferromagnetic interactions between the Co(II) ions of the metal core of compound **1** and **2**

The Co-O-Co angles vary in the range $95\text{-}105.2^\circ$ for compound **1** and $95.9^\circ\text{-}99.4^\circ$ for compound **2**. According to the literature and the experimental data the global exchange interaction between the magnetic orbitals is ferromagnetic.[15] In addition in compound **2** there are two *end-on* R-phenylcyanamides with Co-N-Co angles close to 100° (101.9° and 101.5°). As we can see in the literature and the experimental data they are related to the ferromagnetic coupling between the Co(II) of compound **2**. [3]

The Co---Co distances range 3.189-3.314 Å for compound **1** and 3.160-3.311 Å for **2**. The Co---Co distances obtained for both compounds are the ones expected for those bridged by O atoms from dpk derivatives that present ferromagnetic coupling.[15], [16]

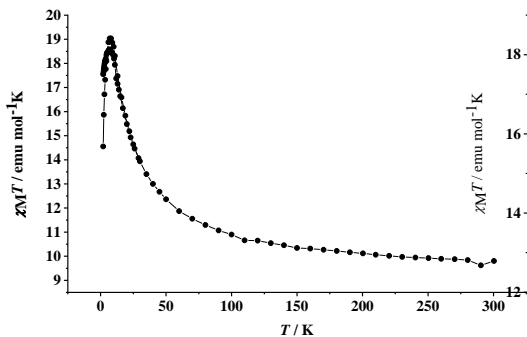


Fig.10 $\chi_M T$ vs T plot for compound **1**

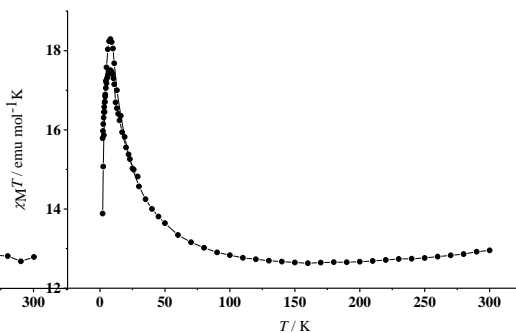


Fig.11 $\chi_M T$ vs T plot for compound **2**

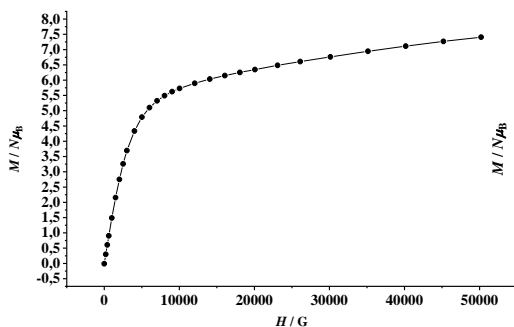


Fig.12. Magnetization vs. magnetic field at 2K for compound **1**

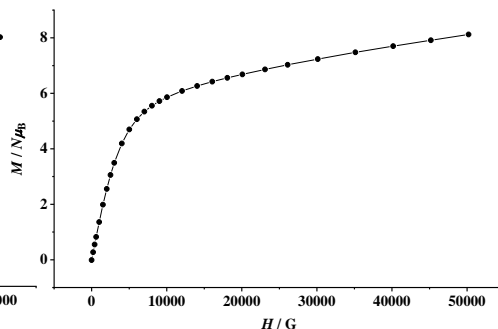


Fig.13. Magnetization vs. magnetic field at 2K for compound **2**

It is difficult to model the magnetic behaviour of a four high-spin Co(II) compound due to the anisotropy of the exchange constants and the spin g-factor.[5], [8] We attempt to present a six J-model that would be used to evaluate the exchange coupling for compound **1** Fig.14. Taking into account the similarity of Co-O-Co angles between Co(3)---Co(4) and Co(1)---Co(2), Co(1)---Co(4) and Co(2)---Co(3), Co(2)---Co(4) and Co(1)---Co(3) we could approximate to a three J-

model, shown in Fig.15, in order to study the exchange coupling. J_2 is referred to the exchange constant through the Co-(μ_3 -OC(OH)py₂)-Co angles which average angle is 97.74°. According to the literature the coupling interaction between Co(2) \leftrightarrow Co(4) and Co(1) \leftrightarrow Co(3) should be ferromagnetic with a positive J_2 value.

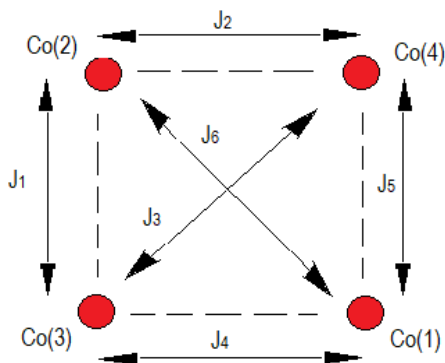


Fig 14. Six J-model to evaluate the exchange coupling for **1**.

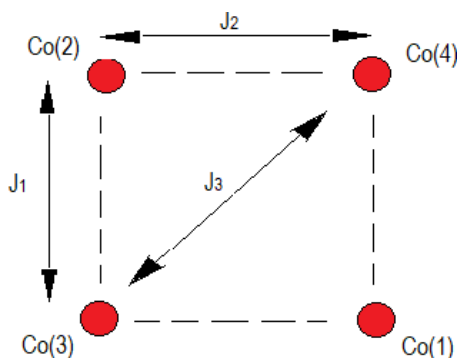


Fig.15. Three J-model to evaluate the exchange coupling for **1**

For compound **2** a four-J model would be used to represent the exchange coupling Fig.16. This model is valid for centrosymmetric dicubanes with the ideal C_{2h} symmetry [8]. J_1 is referred to the exchange constant through the Co-(μ_3 -OC(OH)py₂)-Co angles (β) and the Co-(μ_2 -OC(OCH₃)py₂)-Co (α). The values of the β angles are 97.64° and 95.89° and the values of the α angles are 99.41° and 98.48°. These superexchange pathways are both ferromagnetic leading to a positive J_1 value. J_2 is referred to the exchange constant through the Co-(μ_2 -R-PhNCN)-Co angles (β') and the Co-(μ_3 -OC(OH)py₂)-Co angles (α'). The values of the β' angles are 101.52°

and 101.89° and the values of the α' angles are 96.95° and 98.84° . These superexchange pathways are both ferromagnetic leading to a positive J_2 value. Lastly, J_3 is referred to the exchange constant through the Co-(μ_3 -OC(OH)py₂)-Co angles with values of 98.27° and 98.78° . These superexchange pathways are also ferromagnetic and lead to a positive J_3 value [4], [5], [8], [13]

For clusters with a Mn(II) or Ni(II) metal core the J values had been calculated using the expression based on the HDVV Hamiltonian Eq.1 in previous published studies.[3], [4], [16] For Ni(II) double cubane complexes with R-PhNCN and dpk as bridging ligands the three J parameters are positive.[3] So we expect the same behaviour for our Co(II) complexes.

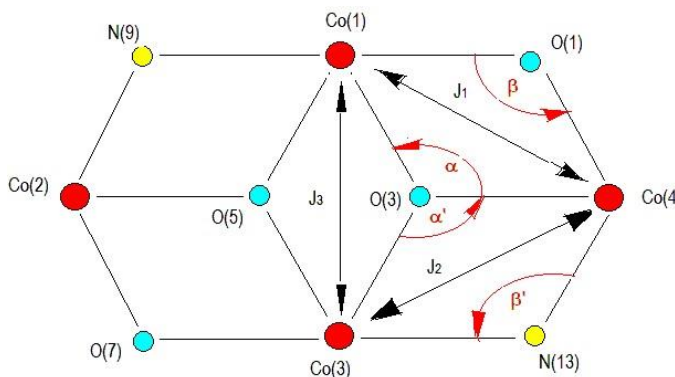
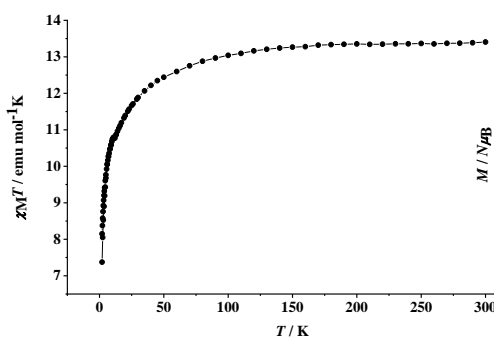
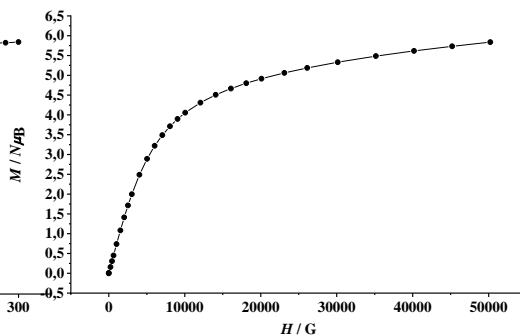


Fig.16. Four J-model to evaluate the exchange coupling for compound **2**.

The χ_{MT} vs. T plot of compound **4** in the 2-300K temperature range is showed at Fig.17 .At 300K compound **4** exhibit a χ_{MT} value of $13.4 \text{ cm}^3 \text{ mol}^{-1} \text{ K}$. This value is lower than the one expected for two isolated Tb(III) atoms which is $23.64 \text{ cm}^3 \text{ mol}^{-1} \text{ K}$. [9] On cooling the sample, χ_{MT} values remain constant up to 100 K. On further cooling χ_{MT} decreases gradually to $2.07 \text{ cm}^3 \text{ mol}^{-1} \text{ K}$ at 35 K. Below that temperature, χ_{MT} values decrease to $7.37 \text{ cm}^3 \text{ mol}^{-1} \text{ K}$ in a short temperature range (35-2 K). This compound shows paramagnetic behaviour. In the range of 300-35 K the Curie's law is obeyed. Below that temperature χ_{MT} values decrease as a consequence of the depopulation of the sublevels generated for the ligand-field effect and the large spin-orbit coupling. The field dependence of magnetization of compound **4** was recorded at 2K as shown in Fig.18 On increasing the external field, M values increase to a maximum value of $5.8 \text{ N}\mu\text{B}$ at 5 T. The saturation value for a two Tb(III) metal ions compound should be $\sim 30 \text{ N}\mu\text{B}$. [9]

Fig.17. $\chi_M T$ vs T plot for compound 4Fig 18. Magnetization vs.magnetic field
at 2K for compound 4

The $\chi_M T$ vs. T plot of compound 5 in the 2-300K temperature range is shown in Fig.19 .At 300K compound 5 exhibits a $\chi_M T$ value of $28 \text{ cm}^3 \text{ mol}^{-1} \text{ K}$. This value is a lot lower than the expected for five isolated Dy(III) ions which is $70.85 \text{ cm}^3 \text{ mol}^{-1} \text{ K}$ [9]. This fact could be for the large anisotropy of the Dy(III) ions in this complex or for the presence of weak antiferromagnetic interactions between the Dy(III) ions.[11] On cooling the sample, $\chi_M T$ values remain constant up to 130 K. On further cooling $\chi_M T$ decreases gradually to $24.7 \text{ cm}^3 \text{ mol}^{-1} \text{ K}$ at 40 K. Below that temperature, $\chi_M T$ values decrease suddenly to $13.09 \text{ cm}^3 \text{ mol}^{-1} \text{ K}$ at 2 K. The distances between the lanthanides ions ($3.512\text{-}3.524 \text{ \AA}$) are short enough to consider an antiferromagnetic exchange interaction though the decrease of $\chi_M T$ values at low temperatures could be for the depopulation of the sublevels generated for the ligand-field effect and the large spin-orbit coupling. The field dependence of magnetization was recorded at 2 K and it's shown in Fig 20. Compound 5 arrives to a saturation value of $10.5 \text{ N}\mu\text{B}$ at 5 T. The saturation value for a five Dy(III) metal ions compound should be $\sim 35 \text{ N}\mu\text{B}$. [9] This fact affirms the large anisotropy of the Dy(III) in this compound.[11]

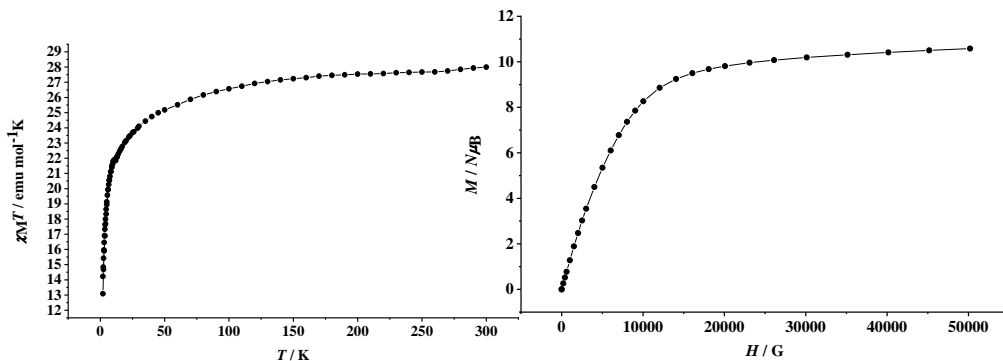
Fig.19. $\chi_M T$ vs T plot for compound 5

Fig.20. Magnetization vs. magnetic field at 2K for compound 5

5.3.1. SMM behaviour.

For compound 1 the ac studies were performed in a dc external magnetic field of 0.1 T in a temperature range of 1.8 to 3.4 K and frequencies of 9.99, 498.67, 852.27, 1250.00 and 1488.09 Hz. The χ_M'' vs. T plot is shown in Fig. 21. And for compound 2 the ac studies were realized in a dc external magnetic field of 0.1 T in a temperature range of 1.8 to 3.4 K and frequencies of 9.99, 199.89, 400.64, 699.63, 997.34 and 1488.09 Hz. The χ_M'' vs. T plot is shown in Fig.22. Both compounds show a dependence of χ_M'' in relation to the oscillating magnetic field frequencies and each plot demonstrates the beginning of a peak at 2K approximately. This experimental data show that the compounds have SMM behaviour though we can't calculate the relaxation time of magnetization because the peak reaches its maximum at very low temperatures and it is not registered into the experimental data.

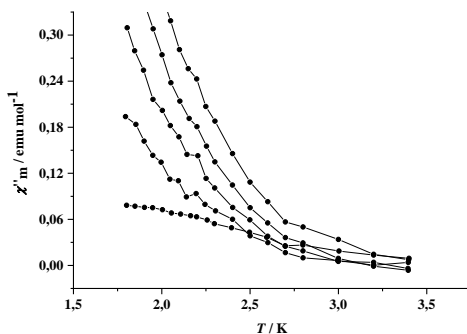


Fig.21 The χ_M'' vs. T plot for compound **1** performed in a dc external magnetic field of 0.1 T in the frequencies of 9.99, 498.67, 852.27, 1250.00 and 1488.09 Hz.

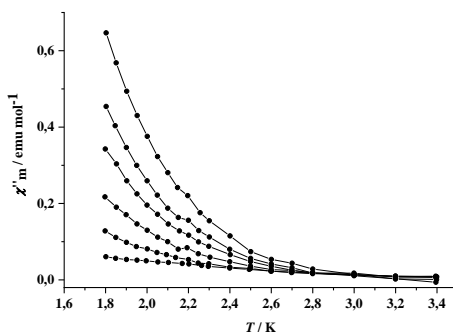


Figure 22. The χ_M'' vs. T plot for compound **2** performed in a dc external magnetic field of 0.1 T in the frequencies of 9.99, 199.89, 400.64, 699.63, 997.34 and 1488.09 Hz

Compound **4** was recorded under a dc external magnetic field of 0 and 0.1 T in a temperature range of 2 to 7 K and frequencies of 9.99 and 997.34 Hz. The χ_M'' vs T plot is shown in Fig. 23. This compound doesn't show a dependence of χ_M'' in relation to the magnetic oscillating field frequencies.

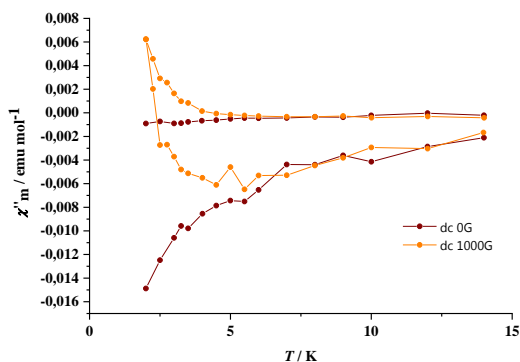


Fig.23. The χ_M'' vs. T plot for compound **4** performed in a dc external field of 0G and 1000 G at 9.99 and 997.34 Hz.

For compound **5** the ac studies were performed in a dc external magnetic field of 0, 0.1 and 0.2 T in a temperature range of 1.99 to 4.99 K and frequencies of 9.99 and 997.34 Hz. The χ_M'' vs. T plot is shown in Fig.24. This compound shows a dependence of χ_M'' in relation to the oscillating magnetic field frequencies and a very low intense peak at 10 K. In order to study the possibility of SMM behaviour and the relaxation time of magnetization we could collect the χ_M'' measurements at higher dc magnetic fields with the objective to obtain more χ_M'' maximum values.

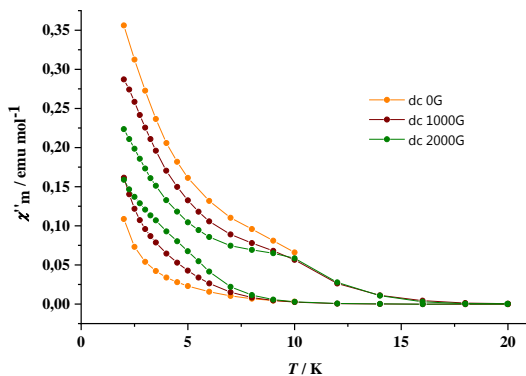


Fig.24. The χ_M'' vs. T plot for compound **5** performed in a dc external field of 0G, 1000 and 2000 G at 9.99 and 997.34 Hz

6. EXPERIMENTAL SECTION

6.1. MATERIALS AND METHODS

All the reagents were used as obtained. The infrared spectra of compounds **1-5** were recorded on a Perkin-Elmer 230-B spectrophotometer.

The magnetic susceptibility and magnetization measurements for compounds **1**, **2**, **4** and **5** were performed with a Quantum Design MPMS-XL SQUID magnetometer at the Magnetic Measurements Unit of the University of Barcelona. Single crystals of **1**, **2**, **3**, **4** and **5** were set up in air on a D8VENTURE (Bruker) diffractometer with a CMOS detector. The crystallographic data and some features of the structure refinements are listed in Tables 1 and 2 of Appendix 2. All the structures were refined by the least squares method. Intensities were collected with a multilayer monochromated Mo-K α radiation. Lorentz polarization and absorption corrections were made in all the samples. The structures were solved by direct methods using the SHELXS-97 computer program and refined by full-matrix least-squares method using the SHEL-2014 computer program. The non-hydrogen atoms were located in successive difference Fourier syntheses and refined with anisotropic thermal parameters on F^2 . Isotropic temperature factors have been assigned as 1.2 or 1.5 times of the respective parent for hydrogen atoms.

6.2. PREPARATION OF THE R-PHENYLCYANAMIDES.

Neutral 4-chlorophenylcyanamide (4-Cl-PhHNCN) and 4-chloro-3-trifluorophenylcyanamide (4-Cl-3-CF₃-PhHNCN) were prepared following the previous published method.[17], [18]

Benzoyl chloride Fig.25A (14.06g, 0.1mol) was added drop-wise to a magnetically stirred solution of ammonium thiocyanate Fig.25B (7.61 g, 0.1 mol) in 100ml of refluxing acetone (boiling at 86°C). Ammonium chloride (white solid) immediately precipitated. After addition was complete, the reaction mixture was allowed to reflux for an additional 10 minutes. Then an acetone solution (100 ml) of the corresponding aniline Fig.25D (0.1 mol) was added drop-wise and the reaction mixture was allowed to reflux for 1h. After that, the reaction mixture was slowly poured into 1500 ml of deionised water with vigorous stirring. The NH₄Cl that precipitated before was dissolved and, simultaneously, the benzoylthiourea Fig.25E derivative (yellow solid) precipitated. The yellowish solid was collected on a Büchner funnel and washed with copious

amounts of water. The wet benzoylthiourea derivative was dissolved in 250 ml of hot 2M aqueous NaOH (20g) solution and then the mixture was brought to a boil (~135°C) for 5 minutes while stirring. While still stirring the reaction mixture was cooled to 60°C. At this temperature lead acetate Fig.25I (0.1 mol, 37.93 g) in 100 ml of water was added to the reaction mixture. The resulting suspension, a deep-black precipitate of PbS formed, was maintained between 50°C and 60°C for 7 minutes. Important note: at temperatures much greater than 60°C and/or longer reaction times after the addition of lead acetate, the product polymerizes. The PbS was filtered off and to the filtrate (colourless solution), cooled in an ice bath, was added approximately 25 ml of glacial acetic acid. The respective R-PhHNCS Fig.25L (white product) immediately precipitates from the solution. The product was collected by filtration and washed with abundant amounts of water and allowed to air dry.

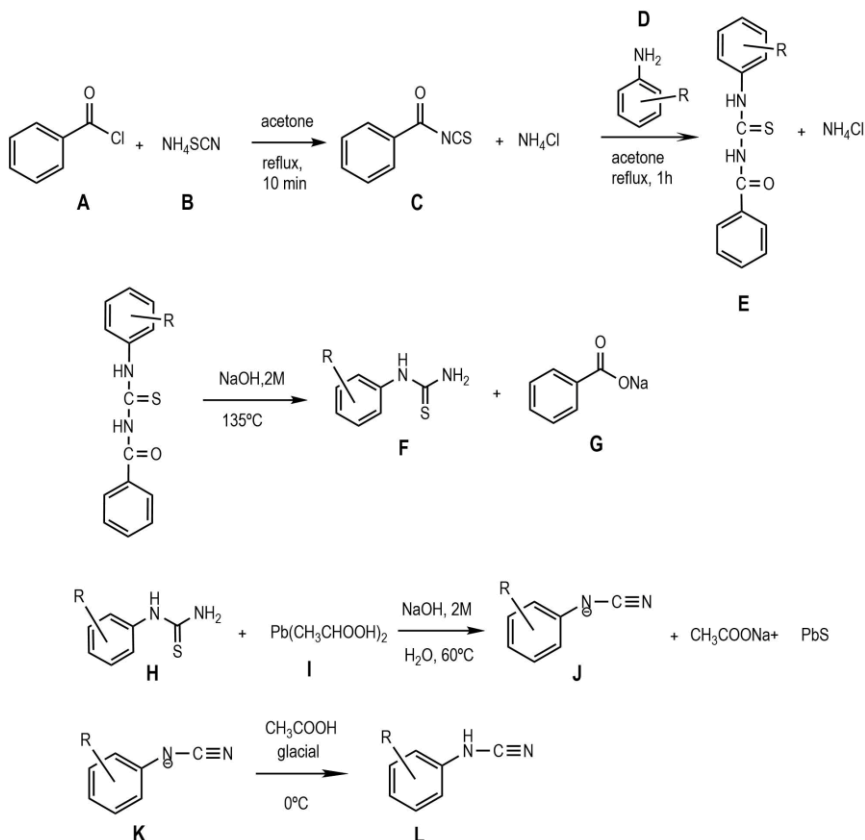
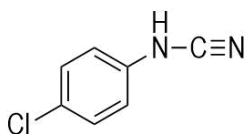
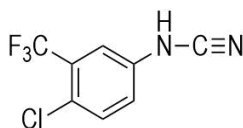


Fig. 25. Reactions that take place on the 4-Cl-PhHNCS (L1) and 4-Cl-3-CF₃-PhHNCS (L2) synthesis.



4-Cl-PhHNCN (**L1**). White powder. Yield (%): 66.4. IR (KBr pellet): 3155-2876, 2237, 1602, 1499 cm^{-1} .



4-Cl-3-CF₃-PhHNCN (**L2**). White powder. Yield (%): 61.3. IR (KBr pellet): 3162-2907, 2243, 1619, 1486 cm^{-1} .

6.3. PREPARATION OF THE METAL COMPLEXES

6.3.1. Preparation of [Co₄(μ₃-py₂C(OH)O)₄(4-Br-3-CF₃-PhNCN)₂(PhCOO)₂] (1)

An ethanol solution (20 ml) containing Co(NO₃)₂·6H₂O (291.03 mg, 1.00 mmol), (py)₂CO (184.20 mg, 1.00 mmol) and Et₃N (101.00 mg, 1.00 mmol) was added to another ethanol solution (20 ml) containing 4-Br-3-CF₃-PhNCN (265.03 mg, 1.00 mmol) and Et₃N (151.50 mg, 1.5 mmol). The deep-red solution was stirred for 30 minutes and then left to stand at room temperature. Single crystals suitable for X-ray diffraction were obtained within a couple days. The crystals were collected by filtration.

Red crystals. Yield(%) 5.6. IR (KBr pellet): 2138, 2069, 1590, 1477, 1059, 767 cm^{-1} . Anal. Calcd (found) for C₇₂H₅₂Br₂Co₄F₆N₁₂O₁₂: C(%), 48.0 (44.5); H(%), 2.9 (2.6); N(%) 9.4 (10.3).

6.3.2. Preparation of [Co₄(μ₂-py₂C(OH)O)₂(μ₃-py₂C(OCH₃)O)₂(μ₂-4-Cl-PhNCN)₂(4-Cl-PhNCN)₂] (2).

A methanol solution (20 ml) containing Co(NO₃)₂·6H₂O (291.03 mg, 1.00 mmol), (py)₂CO (184.20 mg, 1mmol) and Et₃N (101.00 mg, 1mmol) was added to another methanol solution (20 ml) containing 4-Cl-PhNCN (152.45 mg, 1mmol) and Et₃N (151,50 mg, 1.5 mmol). The deep-red solution was stirred for 30 minutes and then left to stand at room temperature. Single crystals

suitable for X-ray diffraction were obtained within a couple days. The crystals were collected by filtration.

Red crystals. Yield(%) 7.8. IR (KBr pellet): 2120, 1584, 1486, 1062, 773 cm^{-1} . Anal. Calcd (found) for $\text{C}_{74}\text{H}_{56}\text{Cl}_4\text{Co}_4\text{N}_{16}\text{O}_8$: C(%) 53.1 (52.4); H(%), 3.3 (3.3); N(%) 13.3 (12.9).

6.3.3. Preparation of $[\text{Co}(\text{py}_2\text{C}(\text{OH})\text{O})(\text{py}_2\text{C}(\text{OCH}_2\text{CH}_3)\text{O})][\text{NO}_3] \cdot 3\text{H}_2\text{O}$ (3).

An ethanol solution (10ml) containing 1,10-phenanthroline (90.11 mg, 0.5 mmol) and another ethanol solution (10 ml) containing $\text{Eu}(\text{NO}_3)_3 \cdot 6\text{H}_2\text{O}$ (223.04 mg, 0.5 mmol) were added to a third ethanol solution (10 ml) containing $\text{Co}(\text{NO}_3)_2 \cdot 6\text{H}_2\text{O}$ (291.03 mg, 1 mmol), $(\text{py})_2\text{CO}$ (368.4 mg, 2 mmol) and Et_3N (202.00 mg, 2 mmol). The deep-red solution was stirred for 30 minutes and then left to stand at room temperature. Single crystals suitable for X-ray diffraction were obtained within a couple days. The crystals were obtained by filtration.

Red crystals. Yield(%) 28. IR (KBr pellet): 1606, 1438, 1014, 770 cm^{-1} .

6.3.4. Preparation of $[\text{Zn}_2\text{Tb}(\mu_2\text{-py}_2\text{C}(\text{OCH}_2\text{CH}_3)\text{O})_3(\mu_3\text{-py}_2\text{C}(\text{OCH}_2\text{CH}_3)\text{O})(\text{NO}_3)(\text{H}_2\text{O})][\text{Tb}(\text{NO}_3)_5]$ (4).

An ethanol solution (10 ml) containing 1,10-phenanthroline (90.11 mg, 0.5 mmol) and another ethanol solution (10 ml) containing $\text{Tb}(\text{NO}_3)_3 \cdot 6\text{H}_2\text{O}$ (226.52 mg, 0.5 mmol) were added to a third ethanol solution (10ml) containing $\text{Zn}(\text{NO}_3)_2 \cdot \text{H}_2\text{O}$ (297.46 mg, 1 mmol), $(\text{py})_2\text{CO}$ (368.4 mg, 2 mmol) and Et_3N (202.00 mg, 2mmol). The yellow solution was stirred for 30 minutes and then left to stand at room temperature. Single crystals suitable for X-ray diffraction were obtained within 10 days. The crystals were collected by filtration.

Yellow crystals. Yield(%) 6.8. IR (KBr pellet): 1600, 1479, 1049, 773 cm^{-1}

6.3.5. Preparation of $[\text{Dy}_5\text{Co}_4(\text{py}_2\text{C}(\text{OH})\text{O})_4(\mu_3\text{-py}_2\text{CO}_2)_4(\mu_4\text{-py}_2\text{CO}_2)_2(\text{O})_2(\text{H}_2\text{O})_6(\text{NO}_3)_2][\text{NO}_3]$ (**5**).

A methanol solution (10 ml) containing 1,10-phenanthroline (90.11 mg, 0.5 mmol) and another methanol solution (10 ml) containing $\text{Dy}(\text{NO}_3)_3 \cdot 6\text{H}_2\text{O}$ were added to a third methanol solution (10 ml) containing $\text{Co}(\text{NO}_3)_2 \cdot 6\text{H}_2\text{O}$ (291.03 mg, 1 mmol), $(\text{py})_2\text{CO}$ (368.4 mg, 2 mmol) and Et_3N (202 mg, 2 mmol). The deep-red solution was stirred for 30 minutes and then left to stand at room temperature. Single crystals suitable for X-ray diffraction were obtained within 30 days. The crystals were collected by filtration and washed with small amounts of hexane.

Red crystals. Yield (%): 9.4%. IR (KBr pellet): 1606, 1442, 1014, 767 cm^{-1} .

7. CONCLUSIONS

The R-phenylcyanamides were obtained as expected with a good reaction yield. For compound **1** and **2** the synthesis method used was similar as previous publications where the final product has a dicubane metal core structure with R-phenylcyanamides as bridging ligands in the *end-on* coordination mode. Only for compound **2** this fact was followed but for **1** the resulting metal core structure was a cubane and not a dicubane as expected. Both compounds show a final ferromagnetic behaviour which is associated with the Co-O-Co angles (O atom from the dpk derivatives) for **1** and **2** and with the Co-N-Co angles (N atom from the R-phenylcyanamide in the end-on coordination mode) for **2**. Therefore we can affirm that there is a relation between the structure of the compound with the magnetic properties where the combination of dpk and R-phenylcyanamides with Co(II) ions lead to a large range of coordination modes and a final ferromagnetic behaviour. Compound **4** consists in a paramagnetic specie with two Tb(III) atoms in the crystal structure. Compounds **3** and **5** were synthesized with the aim of obtaining heteronuclear metallic clusters with R-phenylcyanamides and dpk derivatives as bridging ligands. The initial Co(II) of both compounds has oxidized along the reaction process to Co(III). Compound **3** consists in a mononuclear molecule with Co(III) therefore is diamagnetic and compound **5** don't present coupling interaction between the Dy(III) and Co(III) metal ions because of the diamagnetic behaviour of Co(III). The dpk derivatives after deprotonation show a large coordination flexibility in all compounds specially in compound **5** where the $\text{py}_2\text{CO}_2^{2-}$ anion

has the $\eta^1:\eta^3:\eta^2:\eta^1:\mu_4$ and $\eta^1:\eta^2:\eta^2:\eta^1:\mu_3$ coordination modes. Compounds **1**, **2**, and **5** show SMM behaviour in a temperature lower than 2K though more magnetic data need to be collected in order to calculate the relaxation time of magnetization.

8. REFERENCES AND NOTES

- [1] A. J. Tasiopoulos and S. P. Perlepes, "Diol-type ligands as central 'players' in the chemistry of high-spin molecules and single-molecule magnets," in *Journal of the Chemical Society, Dalton Transactions*, no. 41, 2008, pp. 5537–5555.
- [2] G. S. Papaefstathiou and S. P. Perlepes, "Families of polynuclear manganese, cobalt, nickel and copper complexes stabilized by various forms of di-2-pyridyl ketone," in *Comments on Inorganic Chemistry*, vol. 23, no. 4, 2002, pp. 249–274.
- [3] S. Speed, B. Casanovas, and R. Vicente, " μ 1,1-R-phenylcyanamido bridges as a new safe synthetic strategy for ferromagnetic molecular clusters," *Dalt. Trans.*, vol. 45, no. 12, pp. 5395–5403, 2016.
- [4] G. S. Papaefstathiou, A. Escuer, C. P. Raptopoulou, A. Terzis, S. P. Perlepes, and R. Vicente, "Defective Double-Cubane, Tetranuclear Manganese (II) and Cobalt (II) Complexes with Simultaneous μ 1, 1 -Azido and μ -O Bridges," no. li, pp. 1567–1574, 2001.
- [5] M. G. Barandika *et al.*, "Ferromagnetic interactions in the first dicubane-type complex involving cyanate ligand: [Co4(dpk-OH)2(dpk-OMe)2(NCO)4]," *Chem. Commun.*, no. 1, pp. 45–46, 2001.
- [6] J. Gispert, Ribas, "Coordination Chemistry," Barcelona: Wiley-VCH verlag GMH & Co. KGaA, Weinheim, 2008, pp. 295–338.
- [7] M. D. Joel S Miller, *Magnetism: Molecules to Materials V*. 2008.
- [8] Z. E. Serna *et al.*, "Dicubane-like tetrameric cobalt(II)-pseudohalide ferromagnetic clusters," *Inorg. Chem.*, vol. 40, no. 18, pp. 4550–4555, 2001.
- [9] D. A. Atwood, Ed., "The Rare Earth Elements," John Wiley & Sons, Ltd, 2012, pp. 153–258.
- [10] J. Long *et al.*, "Dysprosium Single-Molecule Magnets with Bulky Schiff-base Ligands: Modification of the Slow Relaxation of the Magnetization by Substituent Change," *Chem. - A Eur. J.*, 2018.
- [11] B. Casanovas, "Compostos de coordinació magnètics i/o luminescents derivats d'elements 3d o 4f: Cercant sistemes multipropietat (Doctoral thesis)," *Dr. Thesis*, pp. 1–312, 2017.
- [12] H. K. Peng *et al.*, "Structure and single-molecule magnet behavior of a rhombus-shaped Dy4 cluster," *Polyhedron*, vol. 157, pp. 316–320, 2019.
- [13] G. S. Papaefstathiou, A. Escuer, M. Font-Bardía, S. P. P. A, X. Solans, and R. Vicente, "Benzoate as terminal ligand in the defective double-cubane, / tetranuclear cobalt(II) complex [Co4(N3)2(O2CPh)2{(py)2C(OH)O}4] \times 2DMF with simultaneous m1,1-azido and m-O bridges / [(py)2C(OH)O? the monoanion of the hydrated, gem-diol form of di-2-pyridyl]," *Polyhedron*, vol. 21, no. 1, pp. 2027–2032, 2002.
- [14] U. Dutta *et al.*, "Synthesis, structure and magnetic properties of nanodimensional La1-xBaxFe0.5Mn0.5O3 perovskites," *J. Alloys Compd.*, vol. 777, pp. 1396–1402, 2019.
- [15] X. F. Ma, Z. Wang, X. L. Chen, M. Kurmoo, and M. H. Zeng, "Ligand Effect on the Single-Molecule Magnetism of Tetranuclear Co(II) Cubane," *Inorg. Chem.*, vol. 56, no. 24, pp. 15178–15186, 2017.
- [16] M.-L. Tong, S.-L. Zheng, J.-X. Shi, Y.-X. Tong, H. K. Lee, and X.-M. Chen, "Synthesis, crystal structures and properties of six cubane-like transition metal complexes of di-2-pyridyl ketone in gem-diol form," in *Journal of the Chemical Society, Dalton Transactions*, no. 8, 2002, pp. 1727–1734.
- [17] A. Escuer, F. A. Mautner, N. Sanz, and R. Vicente, "New examples of the unusual X-phenylcyanamido bridging ligands. Crystal structure and magnetic properties of MnII derivatives," *Polyhedron*, vol. 23, no. 8, pp. 1409–1417, 2004.
- [18] H. Brand, P. Mayer, A. Schulz, T. Soller, and A. Villinger, "Synthesis and structure of monomeric, trimeric, and mixed phenylcyanamides," in *Chemistry - An Asian Journal*, vol. 3, no. 6, 2008, pp. 1050–1058.

9. ACRONYMS

Dpk: 2-pyridil ketone.

R-PhHNCN: R-phenylcyanamide in the neutral form

R-PhNCN: R-phenylcyanamide in the anion form.

SMM: single molecule magnet..

APPENDICES

APPENDIX 1: IR SPECTRA

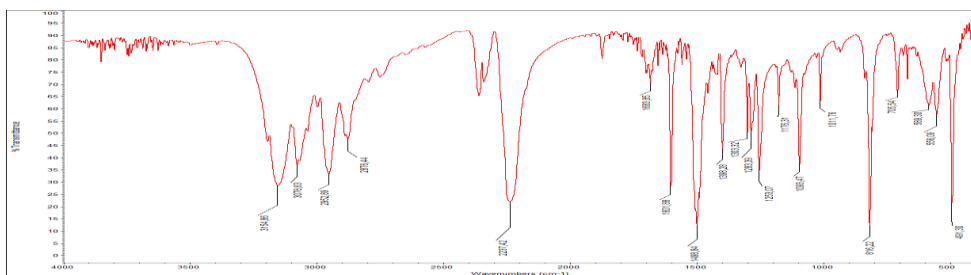


Fig.1(Apx1). IR spectrum of 4Cl-PhNCN (L1)

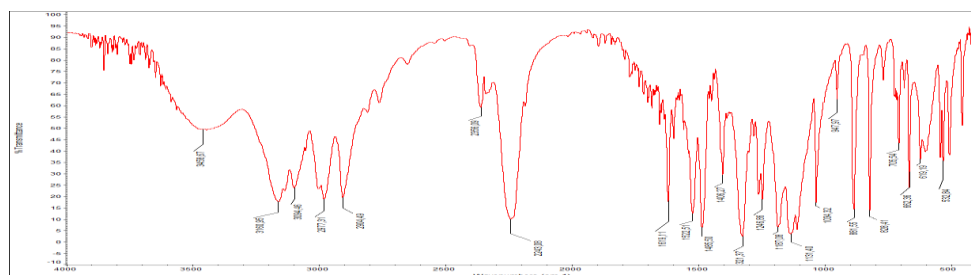


Fig.2(Apx1). IR spectrum of 4Cl-3CF₃-PhNCN (L2)

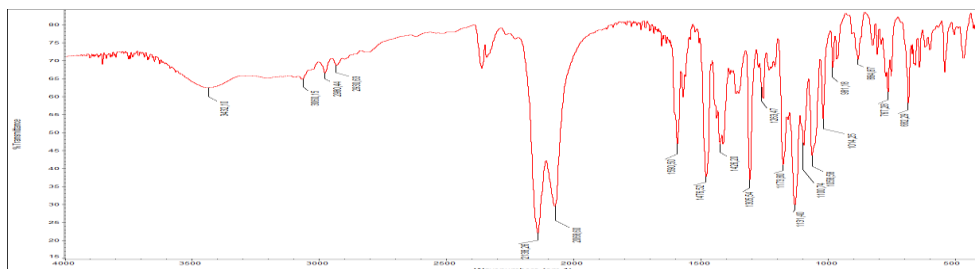


Fig.3(Apx.1). IR spectrum of compound (1)

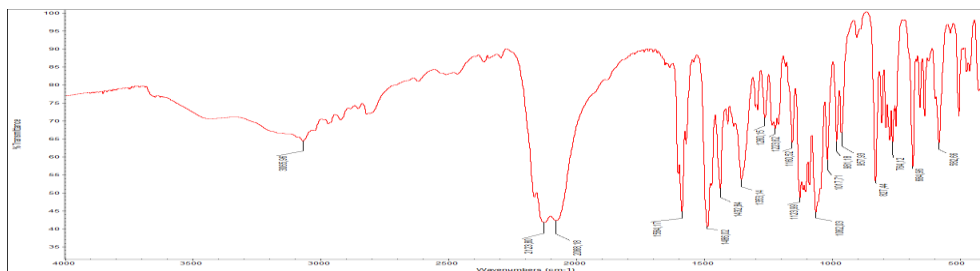


Fig.4(Apx.1). IR spectrum of compound (2).

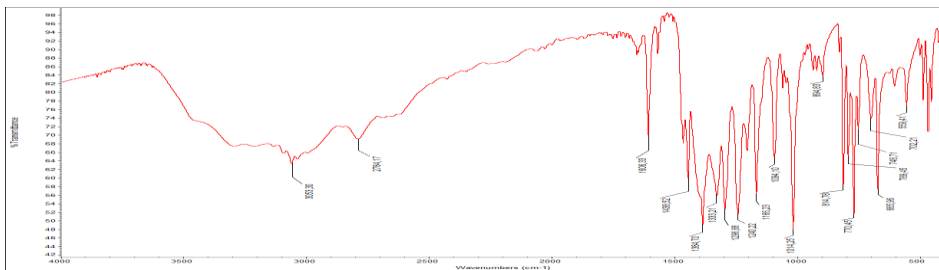


Fig.5(Apx1) IR spectrum of compound (3)

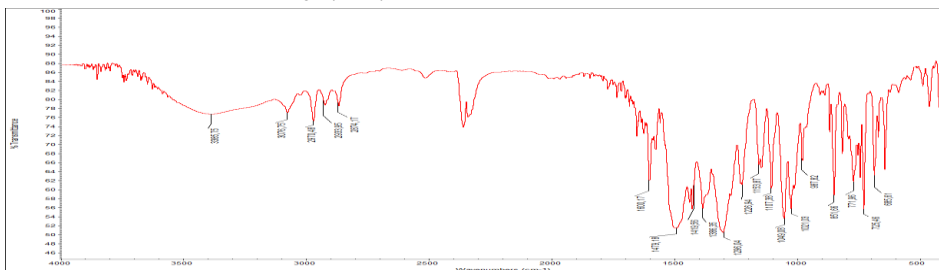


Fig.6(Apx1) IR spectrum of compound (4)

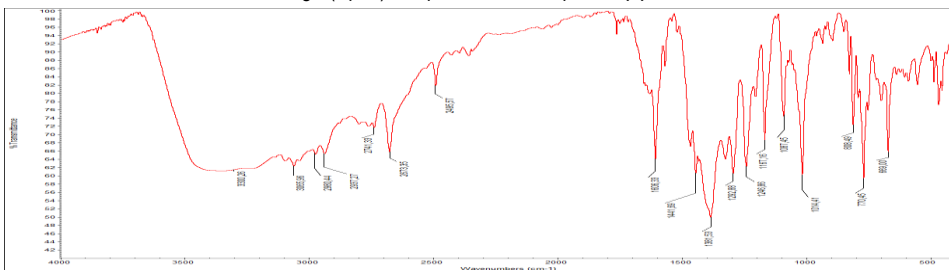


Fig.7(Apx.1) IR spectrum of compound (5)

APPENDIX 2: CRISTAL DATA AND SELECTED BOND LENGTHS AND ANGLES FOR COMPOUNDS 1-5.

Crystal Data	Compound 1	Compound 2	Compound 3
Formula	C ₇₄ Br ₂ Co ₄ F ₆ N ₁₂ O ₁₂	C ₇₄ H ₅₆ C ₁₄ Co ₄ N ₁₆ O ₈	C ₂₄ Co N ₄ O ₄ , N O ₃ , 3(O)
FW [g/mol]	1774.38	1672.05	577.22
Crystal System	monoclinic	monoclinic	monoclinic
Space Group	P21/n (No. 14)	P21/n (No. 14)	577.22
a [Å]	21.853(2)	21.9771(8)	13.0173(5)
b [Å]	15.3405(14)	16.5948(6)	11.9688(4)
c [Å]	25.163(3)	22.3808(8)	16.1303(7)
α[deg]	90	90	90
β [deg]	104.120(3)	100.604(1)	102.986(1)
γ [deg]	90	90	90
V [Å ³]	8180.7(14)	8023.0(5)	2448.85(16)
Z	4	2	4
ρ _{calc} [g/cm ³]	1441	1506	1.566
μ(MoKa) [mm ⁻¹]	1851	1018	0.769
F(000)	3456	3732	1144
Crystal Size [mm]	0.00 x 0.00 x 0.00	0.00 x 0.00 x 0.00	0.00 x 0.00 x 0.00

Table 1(Apx.2). Crystal Data and Details of the Structure Determination of compounds 1, 2 and 3

Crystal Data	Compound 4	Compound 5
Formula	C ₅₂ H ₅₂ N ₉ O ₁₂ Tb Zn ₂ , N ₅ O ₁₅ Tb	C ₁₁₀ H ₈₀ Co ₄ Dy ₅ N ₂₂ O ₃₄ , 2(N O ₃)
FW [g/mol]	1753.67	3426.21
Crystal System	monoclinic	orthorhombic
Space Group	C2/c (No. 15)	Pccn (No. 56)
a [Å]	12.0338(12)	9.9175(7)
b [Å]	21.645(2)	23.6431(8)
c [Å]	55.538(5)	30.7117(10)
α[deg]	90	-
β [deg]	94.956(2)	-
γ [deg]	90	-
V [Å ³]	14412(2)	14462.5(8)
Z	4	4

ρ_{calc} [g/cm ³]	1.461	1.734
μ (MoKa) [mm ⁻¹]	2.507	3.092
F(000)	6304	7376
Crystal Size [mm]	0.00 x 0.00 x 0.00	0.00 x 0.00 x 0.00

Table 2(Apx.2). Crystal Data and Details of the Structure Determination of compounds 4 and 5

atoms	distances [Å]	atoms	distances [Å]	atoms	distances [Å]
Co1-N1	2.0170(2)	Co2-O1	2.1094(3)	Co3-O3	2.1100(3)
Co1-N5	2.1699(3)	Co2-O11	2.0528(2)	Co3-O5	2.0275(2)
Co1-N8	2.1081(3)	Co2-O3	2.0642(2)	Co4-N12	2.1592(3)
Co1-O1	2.0463(2)	Co2-O7	2.1992(3)	Co4-N9	2.1181(3)
Co1-O5	2.2015(3)	Co3-N3	2.0260(2)	Co4-O3	2.2032(3)
Co1-O7	2.1212(3)	Co3-N6	2.0945(2)	Co4-O5	2.1232(3)
Co2-N10	2.1348(3)	Co3-N7	2.1861(3)	Co4-O7	2.0210(2)
Co2-N11	2.1506(3)	Co3-O1	2.2583(3)	Co4-O9	2.0486(2)

Table 3(Apx.2). Selected bond lengths for compound 1

atoms	distances [Å]	atoms	distances [Å]	atoms	distances [Å]
Co1 - N1	2.090(4)	Co2 - N7	2.168(4)	Co3-O5	2.042(3)
Co1 - N3	2.152(4)	Co2 - N9	2.169(4)	Co3-O7	2.145(3)
Co1 - N9	2.094(4)	Co2 - O5	2.223(3)	Co4-N13	2.117(4)
Co1 - O1	2.164(3)	Co2 - O7	2.038(3)	Co4-N15	2.043(5)
Co1 - O3	2.028(3)	Co3 - N13	2.098(4)	Co4-N2	2.161(4)
Co1 - O5	2.136(3)	Co3 - N6	2.142(4)	Co4-N4	2.117(5)
Co2 - N11	2.015(5)	Co3 - N8	2.101(4)	Co4-O1	2.036(3)
Co2 - N5	2.110(5)	Co3 - O3	2.133(3)	Co4-O3	2.226(3)

Table 4(Apx.2) Selected bond lengths for compound 2

atoms	distances [Å]	atoms	distances [Å]	atoms	distances [Å]
Co1 - N1	1.9360(1)	Co1 - N3	1.9378(1)	Co1 - O4	1.8848(1)
Co1 - N2	1.9158(1)	Co1 - N4	1.9132(1)	Co1 - O1	1.8931(1)

Table 5(Apx.2). Selected bond lengths for compound 3

atoms	distances [Å]	atoms	distances [Å]	atoms	distances [Å]
Tb1 - N1	2.58(2)	Tb2 - O14	2.506(17)	Zn1-O1	2.057(12)
Tb1 - N3	2.63(2)	Tb2 - O14_a	2.506(17)	Zn1-O5	2.033(13)
Tb1 - O1	2.295(15)	Tb2 - O16	2.341(17)	Zn1-O7	2.211(13)
Tb1 - O10	2.514(15)	Tb2 - O16_a	2.341(17)	Zn2-N4	2.149(18)
Tb1 - O12	2.306(16)	Tb2 - O17	2.40(2)	Zn2-N6	2.200(17)
Tb1 - O3	2.290(15)	Tb2 - O17_a	2.40(2)	Zn2-N8	2.107(18)
Tb1 - O7	2.348(11)	Tb2 - O19	2.47(2)	Zn2-O3	2.031(17)
Tb1 - O9	2.432(17)	Tb2 - O19_a	2.47(2)	Zn2-O5	2.029(13)
Tb2 - N14	2.66(4)	Zn1 - N2	2.162(16)	Zn2-O7	2.459(13)
Tb2 - O13	2.45(2)	Zn1 - N5	2.06(2)	Zn3-Zn3_b	1.668(5)
Tb2 - O13_a	2.45(2)	Zn1 - N7	2.092(17)		

Table 6(Apx.2). Selected bond lengths for compound **4**. Symmetry transformations used to generate equivalent atoms: (_a) 1-x, y, 1/2-z and (_b) 1-x, 1-y, -z.

atoms	distances [Å]	atoms	distances [Å]	atoms	distances [Å]
Co1 - N5	1.941(7)	Dy1 - N10_a	2.570(7)	Dy2 - O6	2.280(5)
Co1 - N6	1.946(7)	Dy1 - O14	2.364(7)	Dy2 - O6_a	2.280(5)
Co1 - N7	1.928(7)	Dy1 - O15	2.377(6)	Dy2 - O9	2.329(6)
Co1 - N8	1.941(7)	Dy1 - O20_a	2.377(5)	Dy2 - O9_a	2.329(6)
Co1 - O5	1.870(5)	Dy1 - O4	2.212(6)	Dy3 - N9	2.557(7)
Co1 - O7	1.893(6)	Dy1 - O5	2.332(5)	Dy3 - O10	2.513(10)
Co2 - N1	1.913(7)	Dy1 - O6	2.511(6)	Dy3 - O11	2.582(10)
Co2 - N2	1.932(7)	Dy1 - O9_a	2.324(6)	Dy3 - O13	2.388(7)
Co2 - N3	1.942(7)	Dy2 - O19	2.429(5)	Dy3 - O19	2.229(6)
Co2 - N4	1.921(7)	Dy2 - O19_a	2.429(5)	Dy3 - O20	2.390(6)
Co2 - O1	1.888(6)	Dy2 - O20	2.398(6)	Dy3 - O3_a	2.349(6)
Co2 - O3	1.877(6)	Dy2 - O20_a	2.398(6)	Dy3 - O4_a	2.482(6)
				Dy3 - O9	2.397(5)

Table 7(Apx.2) Selected bond lengths for compound **5**. Symmetry transformations used to generate equivalent atoms: (_a) 1/2-x, 1/2-y,

